Bulletin of the Seismological Society of America, Vol. 104, No. 1, pp. –, February 2014, doi: 10.1785/0120130045

Frequency-Dependent Seismic Attenuation in the Eastern United States as Observed from the 2011 Central Virginia Earthquake and Aftershock Sequence

by Daniel E. McNamara, Lind Gee, Harley M. Benz, and Martin Chapman

Abstract Ground shaking due to earthquakes in the eastern United States (EUS) is felt at significantly greater distances than in the western United States (WUS) and for some earthquakes it has been shown to display a strong preferential direction. Shaking intensity variation can be due to propagation path effects, source directivity, and/or site amplification. In this paper, we use S and Lg waves recorded from the 2011 central Virginia earthquake and aftershock sequence, in the Central Virginia Seismic Zone, to quantify attenuation as frequency-dependent $Q(f)$. In support of observations based on shaking intensity, we observe high Q values in the EUS relative to previous studies in the WUS with especially efficient propagation along the structural trend of the Appalachian mountains. Our analysis of $Q(f)$ quantifies the path effects of the northeast-trending felt distribution previously inferred from the U.S. Geological Survey (USGS) "Did You Feel It" data, historic intensity data, and the asymmetrical distribution of rockfalls and landslides.

Introduction

The M_w 5.8 central Virginia earthquake occurred on 23 August 2011 (17:51:04 UTC; depth 6 km) and was felt from southeastern Canada to Florida along the eastern seaboard and west as far as Wisconsin and western Tennessee. The reverse-faulting earthquake had a compound rupture process with three known subevents and occurred on a northeast-striking plane within a region of diffuse seismicity known as the Central Virginia Seismic Zone (CVSZ) (Kim and Chapman, 2005; Horton and Williams, 2012; Chapman, 2013). Ground shaking associated with the 2011 central Virginia earthquake was felt over a larger region than any previous instrumentally recorded earthquake in the eastern United States (EUS) due to efficient energy propagation through crystalline bedrock that underlies much of the eastern margin of the United States (Frankel *et al.*, 1996; Atkinson, 2004). Earthquakes in the central United States (CUS) and EUS are less frequent, but typically felt, and cause damage over a much broader region than equivalent events in the United States west of the Rocky Mountains.

The 2011 central Virginia earthquake produced shaking sufficient to close two nuclear power plants in Virginia with reported shaking levels at the North Anna power plant, 20 km from the epicenter, reaching a factor of two times the maximum design limit (Earthquake Engineering Research Institute [EERI], 2011). A strong-motion accelerometer at the North Anna nuclear power plant recorded the closest known ground motions of the earthquake, in which the maximum horizontal acceleration was 0.27g (Chapman, 2013). The next nearest recording is available from the U.S. Geological Survey (USGS) Advance National Seismic System (ANSS) station US.CBN, in Corbin, Virginia (Table 1), 57 km from the epicenter. Horizontal acceleration, at US.CBN, reached 0.135g. Figure 1 shows the mainshock peak ground accelerations (PGA) plotted against ground-motion prediction equations (GMPEs) determined by Frankel *et al.* (1996) and Atkinson (2004) for eastern North America. The scatter observed in the individual PGAs is likely due to local site effects. The GMPEs are computed assuming hard-rock site conditions. At distances greater than 200 km, the model by Frankel *et al.* (1996) is roughly consistent with the observed PGAs whereas the model of Atkinson (2004) is low. At distances less than 200 km, both models predict lower than observed PGA, however, the paucity of local observations limits our ability to evaluate near-field strong ground motion.

Figure 2a is a record section of the 23 August 2011 M_w 5.8 central Virginia earthquake (17:51:04 UTC, M_w 5.8) recorded at permanent stations in the ANSS backbone and regional networks (US, IU, TA, LD, CO, ET) (Table 1). The closest broadband seismic station was US.CBN, 57 km from the epicenter. The next closest was US.BLA, over 200 km from the epicenter. Because of the limited number of local seismic stations (< 200 km), recordings of the mainshock are not very useful for modification of existing GMPEs in the EUS

Table 1
Seismic Stations Used in This Study

NET.STATION	Latitude (°)	Longitude (°)
CO.JSC	34.2818	−81.2597
ET.CPCT	35.4500	−84.5220
ET.SWET	35.2160	−85.9320
GS.CVRD	38.0686	−77.8081
GS.LWRD	38.0771	−77.7501
GS.ORRD	38.0442	−77.7908
GS.PTRD	38.1196	−77.6227
GS.SPFD	38.1353	−77.5211
GS.SPRD	38.0234	−77.8800
IU.SSPA	40.6358	−77.8876
IU.WVT	36.1297	−87.8300
NM.BLO	39.1719	−86.5222
NM.GLAT	36.2690	−89.2880
NM.HALT	35.9110	−89.3400
NM.HBAR	35.5550	−90.6570
NM.MGMO	37.1540	−92.2687
NM.MPH	35.1230	−89.9320
NM.OLIL	38.7338	−88.0991
NM.PARM	36.6640	−89.7520
NM.SLM	38.6361	−90.2364
NM.UALR	34.7751	−92.3429
NQ.WNC	38.9305	−77.0716
PE.NCAT	36.0790	−79.7712
PE.PAGS	40.2278	−76.7221
PE.PSUB	39.9274	−75.4514
TA.KMSC	35.1420	−81.3333
TA.M54A	41.5079	−79.6647
TA.N54A	40.9617	−79.9892
TA.N59A	40.9168	−75.7703
TA.O56A	40.2683	−78.5663
TA.TIGA	31.4389	−83.5898
TA.W40A	35.1923	−93.0693
US.BLA	37.2113	−80.4205
US.CBN	38.2046	−77.3732
US.CNNC	35.2393	−77.8901
US.ERPA	42.1175	−79.9891
US.GOGA	33.4112	−83.4666
US.MCWV	39.6581	−79.8456
US.NHSC	33.1067	−80.1778
US.TZTN	36.5439	−83.5490
YC.IP01	37.9572	−77.9112
YC.IP02	37.8992	−77.8415
YC.IP03	38.0205	−78.0147
YC.IP04	38.0922	−78.0942
YC.IP05	37.8303	−77.7557
YC.IP06	37.9334	−77.9815
YC.IP07	37.9185	−78.0296

(Atkinson and Boore, 1995). Instead, propagation paths to stations are most prevalent at regional distances (> 200 km) at which the *Lg* wave is dominant and ideally suited for the study of frequency-dependent $Q(f)$ and other regional propagation effects.

In the days following the event, portable seismic stations were deployed by multiple organizations, making this among the best-recorded aftershock sequences in the EUS (Chapman 2013; McNamara *et al.*, 2014). Figure 2b is a record section of an aftershock that occurred on 1 September 2011 (01:09:09 UTC, M_w 3.4) and was recorded at permanent stations in the ANSS backbone and regional networks as well as temporary stations deployed shortly after the mainshock (Table 1). Aftershocks recorded during the deployment offer a unique opportunity to also study seismic attenuation characteristics using *S* waves recorded at local distances (< 200 km), and *Lg* waves at regional distances (> 200 km), in the intraplate setting of the EUS and compare the results with the distinctly different geologic environment of the tectonically active western United States (WUS).

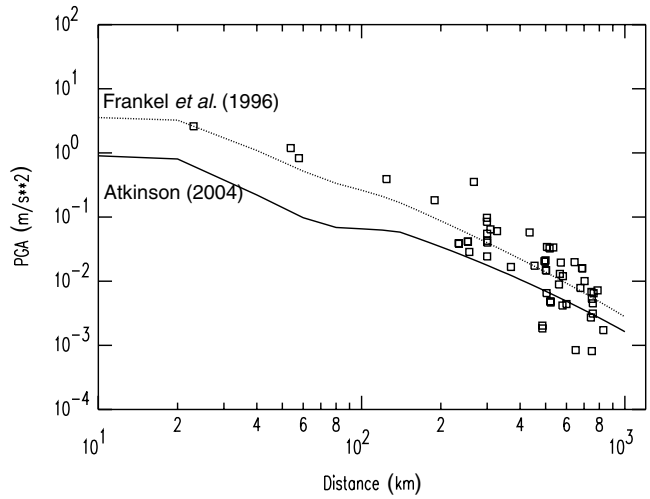

Figure 1. Instrumentally observed horizontal component PGAs (squares) from the 23 August 2011 (17:51:04 UTC) M_w 5.8 Mineral, Virginia, earthquake, recorded at strong-motion stations in the region and used in the USGS Shakemap system. PGAs are compared to the ground-motion prediction equations (GMPEs) of the Frankel *et al.* (1996) and Atkinson (2004) models for eastern North America.

An interesting and persistent feature of the shaking associated with the 2011 M_w 5.8 central Virginia earthquake is a clear preferential direction of the felt reports, with stronger shaking trending to the northeast toward the large urban population centers of Washington, D.C. Hough (2012) concludes from the analysis of shaking intensity residuals that the effects of preferred propagation direction and source directivity together serve to influence shaking by as much as 1.0–1.2 Mercalli intensity units, with roughly comparable contributions from each effect. Similar apparent efficiency of seismic energy propagation, along the strike of the tectonic fabric associated with the Appalachian mountains, has been observed in previous EUS earthquakes. Specifically, the 20 November 1969, Elgood, West Virginia, earthquake produced efficient southwest transmission of energy relative to azimuths perpendicular to the tectonic fabric of the Appalachians (Bollinger and Hopper, 1970). The extensive damage in the Washington, D.C. area, ~200 km from the 2011 central Virginia earthquake, may be due in part to energy from Moho bounce arrivals which have been inferred from previous observations to contribute significantly to strong shaking at distances of 70–200 km in eastern North America (Atkinson, 2004). The Moho bounce effect, however, does not account for the preferred orientation of felt reports and strong ground shaking. To address and

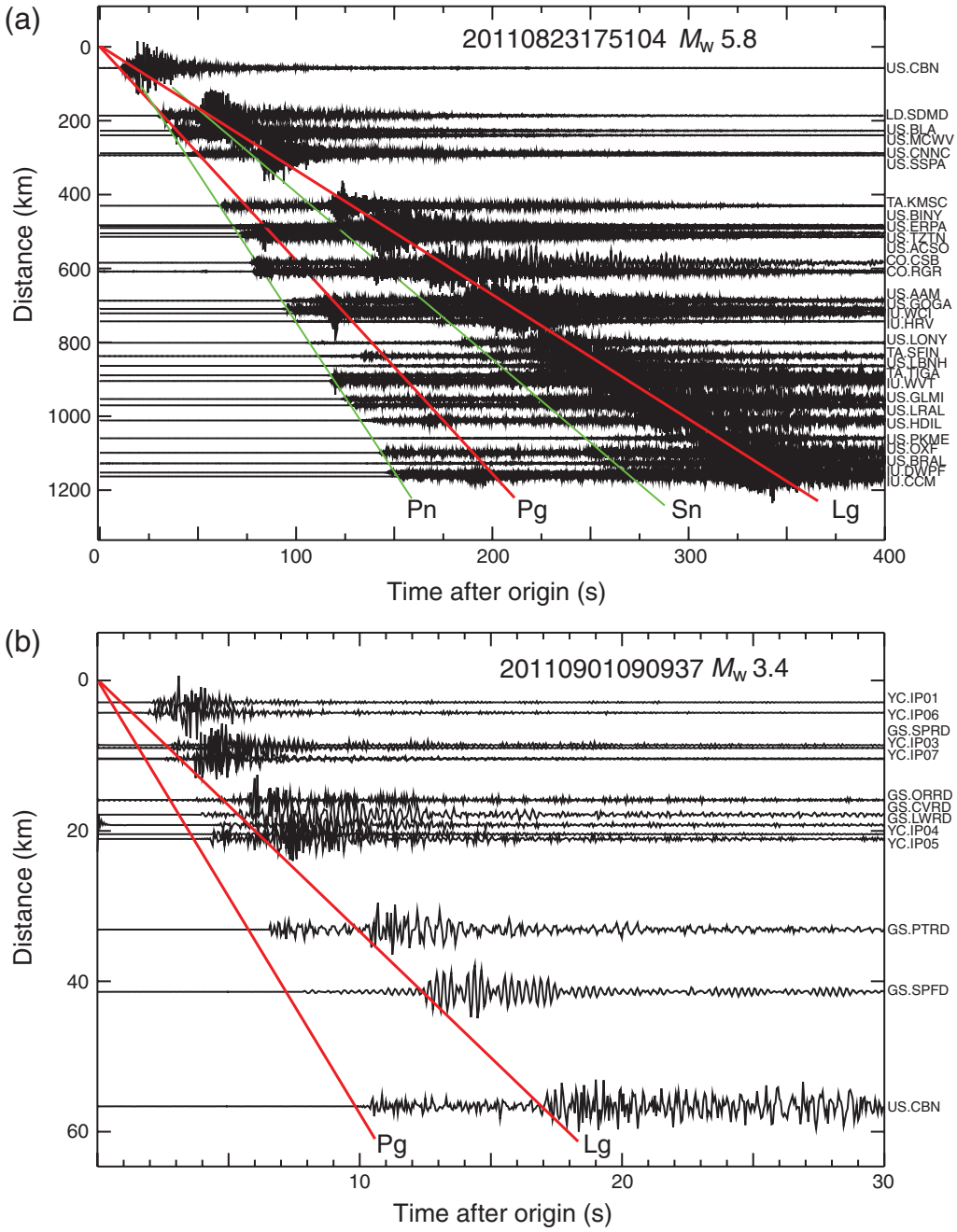

Figure 2. (a) Record section of the 23 August (17:51:04 UTC, M_w 5.8) Mineral, Virginia, earthquake recorded at permanent stations in the ANSS backbone and regional networks (US, IU, TA, LD, CO, ET) networks (201108231751; Table 2). (b) Record section of a large aftershock (M_w 3.4) recorded at both permanent and portable aftershock stations (201109010909; Table 2). BHN, HHN, and BH2 components of motion with a 1 Hz high-pass filter applied are shown. The IASPI 91 model travel times are shown for *Pn*, *Pg*, *Sn*, *Sg*, and *Lg*.

quantify the potential hazard associated with the observation of azimuthally dependent shaking, we investigate frequency-dependent $Q(f)$ in the CVSZ and EUS using regional distance *Lg*- and local *S* waves from the M_w 5.8 mainshock and nearly one year of aftershocks (McNamara *et al.*, 2014).

The attenuation of shear-wave energy is inversely proportional to Q, a dimensionless parameter that describes the energy loss per cycle of oscillation (e.g., Knopoff, 1964). In this document we present our study of the attenuation $(1/Q)$ characteristics of the crust near the CVSZ and the surrounding EUS region (Fig. 2). $Q(f)$ is an important physical parameter that is required for successful simulation of strong ground motion using techniques such as semi-empirical modeling (Joshi and Midorikawa, 2004), composite source modeling (Zeng *et al.*, 1994), and stochastic simulation (Boore, 1983; Rezaeian and Der Kiureghian, 2008, 2010) and more recently with ray-based tomographic methods that solve for 3D Q (Pasyanos *et al.*, 2009; Pasyanos, 2011).

Table 2
Earthquakes Used in This Study

Event ID (yyyy/mm/dd/hh:mm)	Latitude (°N)	Longitude (°E)	Depth (km)	Magnitude (M_l)
2009/07/01/13:44	39.64	−75.48	5	2.8
2009/07/04/12:24	37.38	−80.75	11	2.8
2009/07/07/03:59	37.64	−77.64	10	2.3
2009/10/25/11:16	40.09	−77.00	0	2.6
2009/10/25/11:21	40.09	−77.00	0	2.8
2009/11/25/22:24	37.57	−78.87	3	2.7
2009/12/20/05:36	40.58	−75.19	3	2.3
2009/12/26/23:53	40.88	−74.55	6	2.0
2010/02/05/10:50	40.72	−74.65	6	1.4
2010/02/21/13:59	40.72	−74.66	5	2.6
2010/02/21/17:31	40.71	−74.68	5	2.3
2010/04/04/09:19	38.62	−80.91	0	3.4
2010/04/29/01:36	38.69	−80.82	0	2.6
2010/04/29/12:38	38.65	−80.87	1	2.7
2010/04/29/23:26	38.72	−80.80	5	2.5
2010/05/07/10:26	38.61	−80.91	0	2.6
2010/05/08/03:03	38.62	−80.91	0	2.4
2010/06/03/12:25	40.09	−76.97	1	2.9
2010/06/06/08:13	40.42	−74.31	5	2.3
2010/07/16/09:04	39.18	−77.29	5	3.4
2010/07/24/09:15	38.67	−80.82	2	2.4
2010/10/02/20:17	37.85	−77.52	19	3.0
2010/10/24/08:12	39.43	−81.36	5	2.8
2010/10/28/18:59	34.92	−81.79	4	2.5
2010/10/30/06:10	37.74	−77.46	4	2.4
2010/10/31/16:53	36.51	−81.72	3	2.9
2010/12/25/18:32	40.86	−74.18	2	2.1
2011/03/21/22:02	34.79	−80.06	0	2.9
2011/03/28/07:26	37.02	−80.78	3	2.5
2011/05/10/08:19	40.01	−74.80	5	1.9
2011/05/28/01:33	40.08	−74.99	4	1.7
2011/06/24/17:15	34.35	−80.61	0	2.3
2011/08/23/17:51	37.94	−77.93	6	5.8
2011/08/23/18:46	37.93	−77.93	0	2.8
2011/08/23/19:20	37.91	−78.00	0	2.2
2011/08/24/00:04	37.91	−77.95	7	3.7
2011/08/24/04:45	37.83	−77.95	0	3.4
2011/08/25/04:06	37.89	−77.96	13	2.5
2011/08/25/05:07	37.94	−77.90	5	3.9
2011/08/25/06:37	37.91	−77.97	0	2.3
2011/08/25/15:27	37.94	−77.90	4	2.4
2011/08/25/23:40	37.90	−77.81	4	2.6
2011/08/26/22:52	37.89	−77.94	0	2.1
2011/08/27/09:02	37.94	−77.99	5	2.0
2011/08/28/20:18	37.93	−77.97	6	2.2
2011/08/29/01:06	37.94	−77.99	4	2.3
2011/08/29/03:15	37.94	−77.99	4	2.3
2011/08/29/03:16	37.93	−77.99	4	2.7
2011/08/29/04:19	37.94	−77.99	4	2.2
2011/08/29/23:39	37.97	−77.93	6	2.1
2011/08/30/03:48	37.91	−77.98	7	2.6
2011/08/30/13:26	37.92	−77.98	5	2.1
2011/08/31/13:44	37.92	−77.88	2	2.1
2011/09/01/09:09	37.95	−77.93	3	3.4
2011/09/05/16:54	37.94	−77.97	5	2.5
2011/09/06/09:03	37.92	−77.88	2	2.1
2011/09/07/05:56	37.96	−77.95	6	2.1
2011/09/16/16:17	37.94	−77.99	4	2.1
2011/09/17/08:33	37.93	−77.99	5	2.0
2011/09/17/15:33	37.92	−77.99	4	2.6

(*continued*)

Table 2 (*Continued*)

Event ID (yyyy/mm/dd/hh:mm)	Latitude (°N)	Longitude (°E)	Depth (km)	Magnitude (M_l)
2011/09/17/18:37	37.97	77.83	3	2.1
2011/09/19/04:58	37.98	−77.83	2	2.0
2011/10/05/06:18	37.94	−77.99	3	2.5
2011/10/09/15:53	37.95	−77.98	3	2.4
2011/10/10/01:04	37.92	−77.97	5	2.2
2011/10/12/16:40	37.94	−77.98	4	3.0
2011/10/19/00:02	37.95	−77.95	3	2.3
2011/11/03/12:50	37.95	−77.97	10	2.3
2011/11/19/20:12	37.94	−77.94	2	2.4
2011/11/20/01:06	37.93	−77.94	5	2.3
2011/11/21/01:17	37.95	−77.97	5	1.9
2011/11/21/05:25	37.94	−78.13	5	2.1
2011/12/03/11:12	37.12	−81.91	1	3.1
2011/12/12/21:57	37.96	−78.00	1	2.0
2011/12/24/07:30	37.92	−78.00	4	2.0
2012/01/08/14:25	37.92	−77.99	4	1.9
2012/01/10/19:38	38.70	−80.97	4	2.8
2012/01/13/23:18	37.88	−77.98	5	2.3
2012/01/18/13:08	37.95	−77.96	1	2.5
2012/01/18/14:19	37.91	−78.00	5	2.0
2012/01/18/21:03	37.93	−77.98	4	2.5
2012/01/30/23:39	37.94	−77.98	3	3.1
2012/02/19/07:12	37.91	−77.98	2	2.7
2012/02/27/01:59	37.78	−77.56	12	1.9
2012/02/28/05:15	37.92	−78.00	3	1.8
2012/03/16/18:30	37.50	−78.17	7	2.3
2012/03/26/03:21	37.91	−77.99	8	3.0
2012/04/03/19:00	37.91	−78.00	6	2.5

The *Lg* phase propagates with a group velocity of about 3.5 km/s, the average crustal shear-wave velocity, and is commonly observed as the dominant phase on high-frequency seismograms at regional distances (e.g., Isacks and Stephens, 1975; McNamara and Walter, 2001). *Lg* is generated by a superposition of higher-mode surface waves (Oliver and Ewing, 1957; Knopoff *et al.*, 1973) or as multiply reflected shear energy in a crustal waveguide (Press and Ewing, 1952; Gutenberg, 1955). Consequently, *Lg* provides a good measure of path-averaged crustal attenuation properties. *Lg* amplitude is sensitive to lateral heterogeneity in the crust; consequently, Q is generally lower for tectonically active regions than for stable continental interiors (Mitchell, 1981; Frankel *et al.*, 1990; Atkinson and Mereu, 1992; McNamara *et al.*, 1996; Benz *et al.*, 1997; McNamara, 2000; Ottemoller, 2002; Erickson *et al.*, 2004). Several mechanisms have been proposed to explain these observations: differences in crustal heterogeneity leading to differences in absorption of high-frequency energy (Aki, 1980), differences in crustal temperature (Frankel *et al.*, 1990), and variations in crustal structures that control elastic wave propagation and scattering (Gregersen, 1984; Kennett, 1986).

Frequency-Dependent Q

Numerous researchers have estimated $Q(f)$ for the Earth's crust throughout the world (e.g., Chavez and Priestly, 1986; Frankel *et al.*, 1990; Atkinson and Mereu, 1992;

McNamara *et al.*, 1996; Benz *et al.*, 1997; Erickson *et al.*, 2004; Garcia *et al.*, 2004). The frequency-dependent quality factor $Q(f)$ is commonly modeled using a power law of the form

$$Q(f) = Q_0(f/f_0)^{\eta}, \tag{1}$$

in which f_0 is a reference frequency (generally 1 Hz), Q_0 is Q at the reference frequency, and η is assumed constant over the frequencies of interest.

Data and Methods

Data Selection

Seismograms used in this study include horizontal component *S* and *Lg* waves from crustal earthquakes recorded at local and regional distances. Events analyzed include the M_w 5.8 central Virginia earthquake of August 2011 and its sequence of aftershocks (Table 2) (McNamara *et al.*, 2014). All waveforms were visually inspected and restricted to well-recorded, crustal earthquakes (depth ≤ 20 km). Data used in this study were digitally recorded at regional broadband stations operated by the USGS Global Seismograph Network (GSN) and the ANSS as well as 47 portable stations deployed shortly after the mainshock (Table 1). Earthquake locations and magnitudes used in this study were obtained from USGS Preliminary Determination of Epicenters (PDE). All waveform data used in this study are archived and available for download from the Incorporated Research Institutions for Seismology (IRIS) Data Management Center (DMC).

Lg- and *S*-wave amplitudes used in the Q inversion were restricted to stations that recorded at least two earthquakes and earthquakes recorded by at least two stations. In addition to the visual inspection, we required a signal-to-noise root mean square (rms) amplitude ratio greater than two, in which the noise amplitude is taken from the *P* wave and *P* coda rather than the noise preceding the *P* wave. This step eliminated very few paths, because *Lg* is the dominant arrival on most regional seismograms, and ensured observations where *Lg* is present at all distances. The rms amplitude for *Lg* was windowed from 3.6 to 3.0 km/s, direct *S* from 4.8 to 3.6 km/s, and the *P* wave and *P* coda was windowed from 8.1 to 4.8 km/s (Fig. 3). Waveforms that passed our signal-to-noise criteria were further processed to obtain spectral amplitude measurements. This process included deconvolution of the instrument-response transfer function from the band-pass-filtered seismogram and then the rms amplitude was measured in five one-octave passbands with center frequencies of 0.75, 1.5, 3, 6, and 12 Hz. After applying the earthquake and waveform selection criteria to over 5000 regional seismograms, over 1500 high-quality waveforms from nearly 100 events recorded at 112 stations remained. Data selection criteria, amplitude measurement procedures, and Q inversion methods used in this study are well described in numerous previous publications (see Benz *et al.*, 1997; Erickson *et al.*, 2004; McNamara *et al.*, 2012). Figure 4 shows regional *Lg* paths that passed the data selection criteria and were used to invert for $Q(f)$.

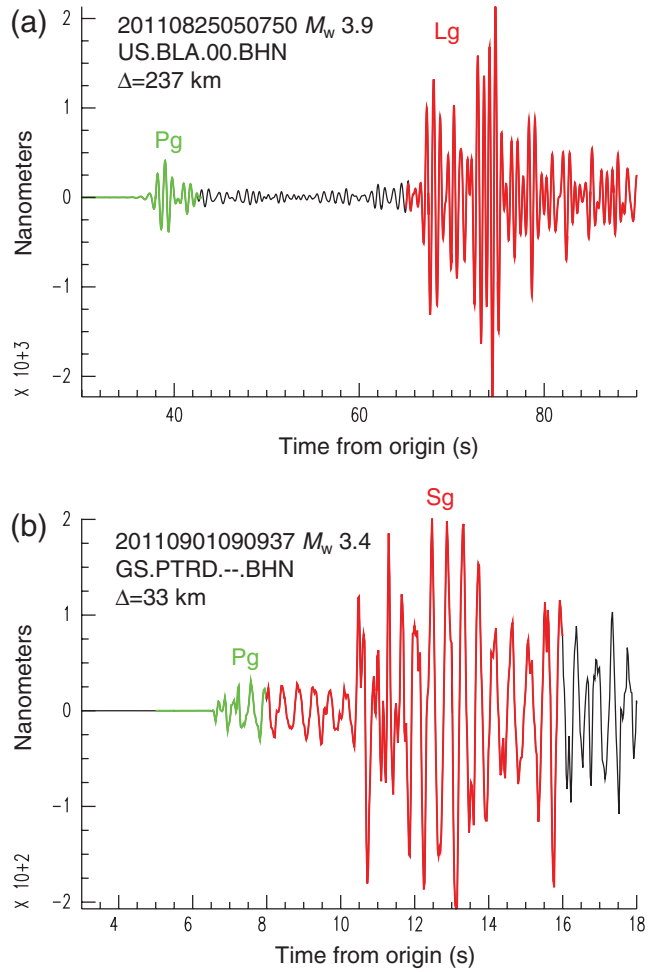

Figure 3. Seismograms of large aftershocks recorded by permanent and portable stations. (a) The largest (M_w 3.9, m_b 4.5) aftershock recorded at US.BLA, 237 km from the epicenter (Table 2, 20110825050750). Windows for signal-to-noise test (green) and *Lg* amplitude (red) measurement are shown. (b) A significant (M_w 3.4) aftershock recorded portable station GS.PTRD, 33 km from the epicenter (Table 2, 20110901090937). Windows for signal-to-noise test (green) and *S*-wave amplitude (red) measurement are shown.

Single Frequency Q Inversion

The individual frequency Q inversion method used in this study is well known and has been applied extensively in numerous tectonic environments. We invert *Lg*- and *S*-wave amplitudes in each frequency band (0.75, 1.5, 3, 6, and 12 Hz) independently using a singular value decomposition algorithm (e.g., Menke, 1980, Aster *et al.*, 2002). The observed amplitude A at frequency f for the jth earthquake recorded at the ith station can be modeled as

$$A_{ij}(f) = R_{ij}^{-\gamma} S_j(f) G_i(f) e^{-\pi f R_{ij}/Q\beta}, \tag{2}$$

in which $S_j(f)$ is the source spectra, $G_i(f)$ is the site amplification, R_{ij} is the epicentral distance between the earthquake j and station i, γ is the exponent for geometrical spreading, Q is the quality factor at frequency f, and β is the average

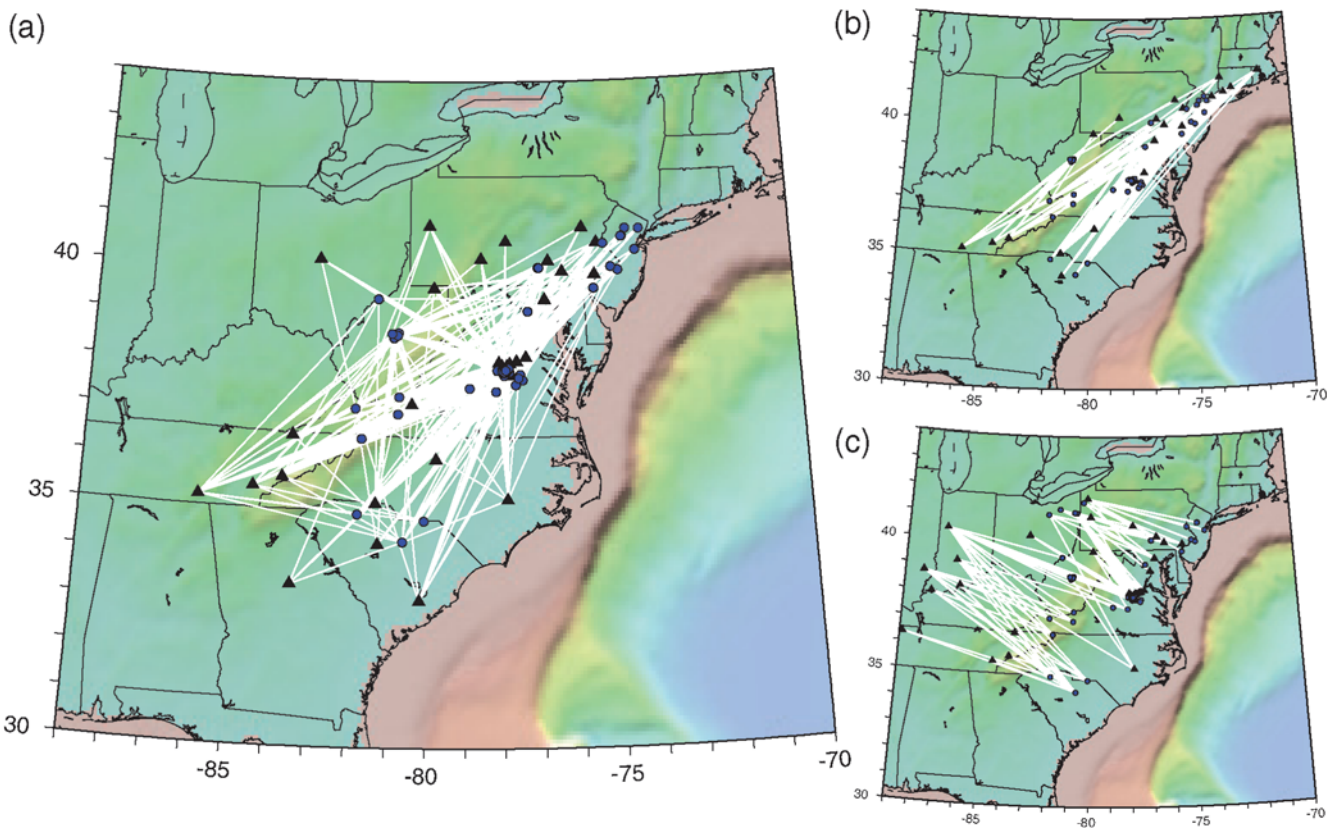

Figure 4. EUS map with portable and permanent regional seismic stations (black triangles) used in this study (Table 1). Earthquakes are shown as blue circles (Table 2). (a) White lines are 1108 *Lg* paths used in the regional average $Q(f)$ inversion. (b) 730 *Lg* paths parallel to strike of Appalachian mountains trending in a northeast–southwest (NESW) orientation. (c) 287 *Lg* paths perpendicular to the Appalachian mountains trending in a northwest–southeast (NWSE) orientation.

shear-wave velocity for the crust. As observed in equation (2), $Q(f)$ is sensitive to several parameters, including the assumption of a shear-wave velocity. Fortunately, this is one of the only parameters for which we have outside information through travel-time and velocity inversions. For this analysis, we assume an average crust shear-wave velocity of 3.6 km/s, which is consistent with a recently refined two-layer crustal velocity model used to locate earthquakes in the CVSZ by the Virginia Tech Seismic Observatory (VTSO; Chapman, 2013). We also assume an average crustal velocity determined from *Sg* travel times recorded using the portable aftershock stations (McNamara *et al.*, 2014).

Taking the logarithm of equation (2) yields the following,

$$\ln A_{ij}(f) + \gamma \ln R_{ij} = \ln G_i(f) + \ln S_j(f) - \pi f R_{ij}/Q\beta. \quad (3)$$

When amplitude corrected for geometric spreading (left side of equation 3) is plotted with respect to distance, the right side of equation (3) describes a line at which the receiver (G_i) and source (S_j) terms control the intercept and the Q term controls the slope. Using a dataset with many source–receiver pairs, a system of linear equations can be set up based on equation (3). The system of equations can be expressed as

$$\boldsymbol{Ax} = \boldsymbol{t}, \quad (4)$$

in which $\boldsymbol{A}$ is the system matrix made up of the parameter coefficients of equation (3), $\boldsymbol{x}$ is a column vector containing the unknown source (S) and receiver (G) terms and the regional Q term, and the $\boldsymbol{t}$ vector comprises the left side of equation (3). The system matrix, $\boldsymbol{A}$, is made up of mostly ones and zeros, with the last column listing a portion of the last term of (3) ($-\pi f R_{ij}/\beta$). We solve for each frequency independently and the known variables are R, f, and β for each source–receiver pair. We solve the matrix inversion for the unknown variables S_j and G_i, as well as a regionally averaged Q for a single frequency passband, with a center frequency f.

By including many earthquake–station pairs, the inversion procedure determines source terms (S_j) for each earthquake j that scale by magnitude, and receiver terms (G_i) for each seismic station i that reflect systematic amplitude contributions due to site-response amplification and/or instrument-response variability. Finally, the inversion solves for a regionally averaged Q for each frequency passband, at center frequencies of 0.75, 1.5, 3, 6, and 12 Hz.

Sensitivity of $Q(f)$ to Geometrical Spreading

Despite the broad acceptance of the frequency-dependent $Q(f)$ model used to describe the attenuation of seismic waves, the cause still remains poorly understood. According to

equation (2), the attenuation of seismic waves as a function of distance in the crust is controlled by: (1) geometrical spreading, $R_{ij}^{-\gamma}$, and (2) the quality factor, Q. Under the effects of geometrical spreading, seismic-wave amplitude is reduced as wave packets spread and thin over distance and time (Morozov, 2008, 2011). Q is an apparent attenuation and can be caused by anelasticity, in which elastic energy is converted to heat, or by scattering from heterogeneities in the crust. Several authors have demonstrated that it is difficult to isolate the contributions of these different mechanisms on Q (Frankel *et al.*, 1990; Frankel, 1991; Mayeda *et al.*, 1992).

A significant problem with the frequency-dependent Q model to describe seismic-wave attenuation is the trade-off between geometrical spreading, γ, and Q. In practice, most studies fix γ for specific wave propagation distances and solve for frequency-dependent Q (Frankel *et al.*, 1996; Atkinson, 2004; McNamara *et al.*, 2012). In contrast, Morozov (2008) proposed a geometrical attenuation model as an alternative to the frequency-dependent $Q(f)$ paradigm that explicitly separates the contributions of geometrical spreading and intrinsic attenuation. In this model of seismic-wave attenuation, the geometrical spreading is assumed variable and frequency dependent, whereas Q is frequency independent and constant for a given region. To resolve this trade-off between γ and Q, outside information about the wave propagation medium is required. For example, with three unknown parameters (Q, η, γ) the attenuation inversion problem becomes overparameterized because only two constraints (amplitude as a function of frequency) are available from the seismic data.

From the perspective of earthquake hazard, it is important to maintain a common standard suitable for comparison of absolute amplitude decay as a function of distance rather than determine the contribution of all parameters which determine the attenuation properties of the Earth. As we have noted, $Q(f)$ is an important physical parameter that has been adopted for the simulation of strong ground motion (Boore, 1983). As a consequence, and because of the need to have a well-defined background on top of which the Q can be measured, numerous studies focusing on determining the regional variation of Q use fixed geometrical spreading models. This paradigm allows for a quantified comparison of attenuation, and therefore earthquake shaking hazard, between different regions. Evaluation of alternative models, such as geometrical attenuation proposed by Morozov (2008), is beyond the scope of this paper. Likewise, the determination of outside information about the wave-propagation medium may allow us to resolve the trade-off between γ and Q. Because the primary objective of this paper is to determine attenuation properties of the crust in order to improve our understanding the earthquake shaking hazard in the EUS, we apply a hybrid approach in which we solve for $Q(f)$ using datasets grouped by path length with different assumptions of geometrical spreading. This assumption is common and supported by several previous studies that described attenuation for the EUS using a hinged-trilinear functional form, in which geometrical spreading varies with epicentral distance.

Atkinson (2004) describes attenuation in eastern North America by parameterizing geometrical spreading as $R^{-1.3}$ to 70 km, as $R^{0.2}$ for 70–130 km, and $R^{-0.5}$ beyond 130 km. Frankel *et al.* (1996) uses a similar form by describing geometrical spreading as $R^{-1.0}$ to 70 km, as R^{0} for 70–130 km, and $R^{-0.5}$ beyond 130 km. This parameterization is interpreted as reflecting changes in the dominant wave type. At close distances, the direct S waves dominate and the attenuation rate is steep. At distances beyond 70 km, the postcritical reflections from the Moho discontinuity join the direct S waves, increasing energy levels and decreasing the attenuation rate. At regional distances, multiple refractions and reflections of the shear waves trapped in the crustal waveguide, Lg, dominate seismic records and the attenuation rate changes to the commonly used form, $R^{0.5}$ (Frankel *et al.*, 1990; Frankel, 1991; McNamara *et al.*, 1996, Benz *et al.*, 1997). Because the Lg amplitude dataset is restricted to relatively long path lengths (250–1100 km), that are beyond the hinge points of previous EUS Q studies, the geometric spreading term, γ, is assumed to remain constant at 0.5 for each frequency. S waves are more complicated in that path lengths cross hinge points at 70 and 130 km. For this reason, S-wave amplitudes were corrected for geometrical spreading, using equation (3), according to the hinged-trilinear functional form described previously (Atkinson, 2004) and then a Q estimate is determined using the corrected S-wave amplitudes.

Results

In this analysis, we solved for $Q(f)$ using several different datasets. Average datasets include Lg paths (distance range of 250–1100 km) and direct S-wave paths (distance range 0–250 km) with ray paths of all orientations. In addition, we subdivided each of the average datasets into path subsets with general orientations to the northwest–southeast (NWSE) and northeast–southwest (NESW) to investigate the contribution of Q to the preferential distribution of intensity observations (Hough, 2012).

To determine frequency-dependent Q, for each Lg- and S-wave path dataset, the inversion procedure solves for an average Q in each of the separate frequency bands. We repeat the inversion over five octaves, with center frequencies of 0.75, 1.5, 3, 6, and 12 Hz, in order to obtain $Q(f)$. A weighted $L1$ norm least-squares regression analysis is then used to fit the frequency-dependent Q function, $Q(f)$ (from equation 1), to the individual frequency Q estimates. Taking the logarithm of both sides of (1) yields

$$\ln Q = \ln Q_0 + \eta \ln(f) - \eta \ln(f_0), \tag{5}$$

in which Q_0 and η are the unknowns to be determined.

Average Regional Lg $Q(f)$ Results

Example horizontal component Lg amplitudes, corrected for the source (S_j) and receiver (G_i) terms are shown in Figure 5a,b for center frequencies 0.75 and 1.5 Hz and the

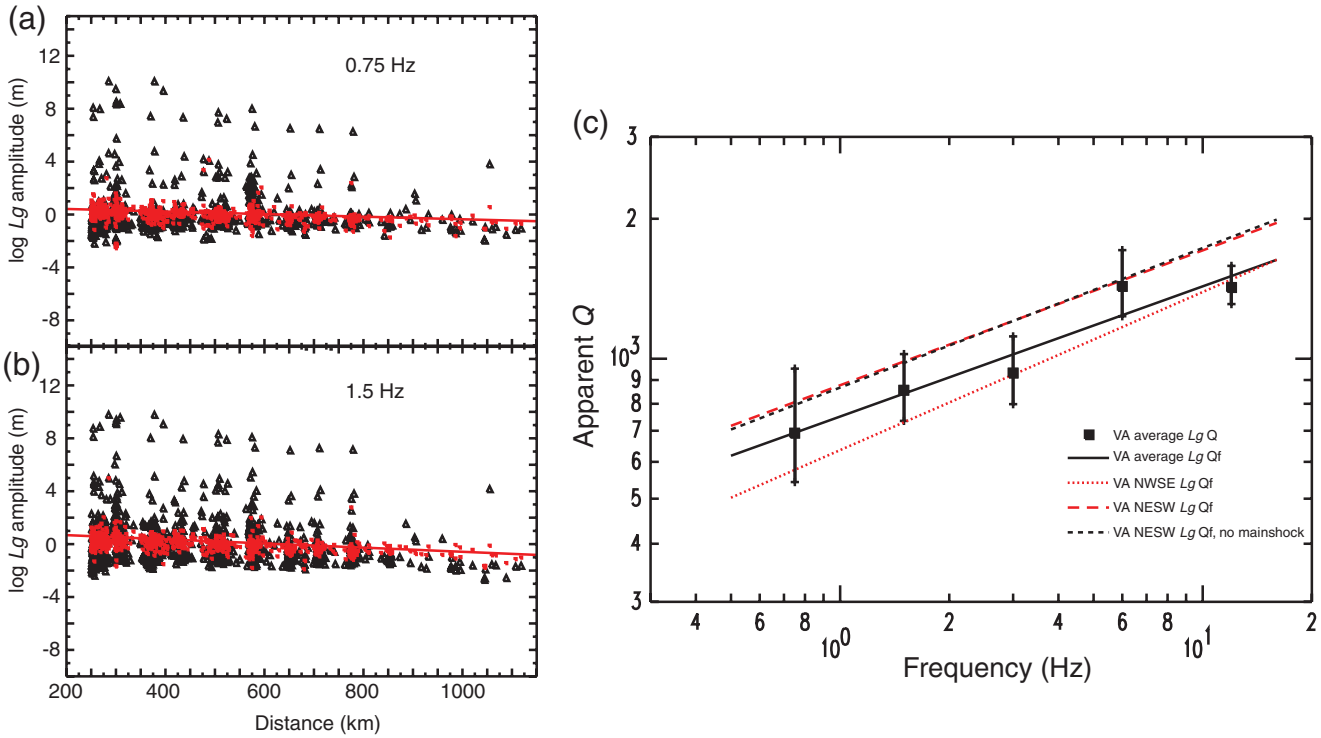

Figure 5. 1108 original horizontal component *Lg* amplitudes (black triangles) and *Lg* amplitudes corrected for source and receiver terms determined in the Q inversion (red squares) are shown. (a) Single frequency Q fits (red lines) for 0.75 Hz and (b) 1.5 Hz. (c) The regional frequency-dependent Q, fit over five passbands, ($Q(f) = 751(\pm 39.0)f^{0.28(\pm 0.054)}$). Plus signs represent the 2σ standard deviation of each Q estimate. $Q(f)$ results for NESW paths ($Q(f) = 877(\pm 41)f^{0.29(\pm 0.050)}$), NWSE paths ($Q(f) = 636(\pm 32)f^{0.34(\pm 0.045)}$), and NESW azimuths with the mainshock removed ($Q(f) = 875(\pm 41.0)f^{0.30(\pm 0.058)}$) are also shown.

straight lines represent the best fitting Q for the particular frequency band using equation (3). In each frequency band, the inversion procedure solves for an average Q using 1108 high-quality *Lg* amplitude observations, from 88 events, recorded at 36 stations, with a distance range of 250–1100 km. After equation (5), we find an average regional *Lg* $Q(f) = 751(\pm 39.0)f^{0.28(\pm 0.054)}$ using the *Lg* ray paths shown in Figure 4a.

Source Terms and Receiver Terms

The terms in equation (2), $S_j(f)$ the source spectra, and $G_i(f)$ the receiver term, are related to the magnitude of the earthquake and any systematic amplitude contributions due to local site response amplification and/or instrument response sensitivity errors, respectively. Figure 6 is a plot of source terms determined in the 1.5 and 6 Hz average *Lg* Q inversions plotted against the magnitude of the earthquake. In general, there is a strong agreement with the size of the source term determined in the Q inversions and the magnitude of the earthquake. This demonstrates that the source terms determined in the inversion are appropriate and contribute to an accurate estimate of Q when corrected from the raw *Lg*- and *S*-wave amplitudes.

Reference Station

Because the instrument response characteristics of all seismic stations used in this study are well known, we expect that receiver terms determined in the Q inversions, $G_i(f)$, will represent the local site amplification at each seismic station, due to soil, bedrock, and vault conditions. Stations used in this study are built into a wide range of site conditions and therefore, experience a wide range of possible site amplification. Most permanent network stations are constructed in vaults blasted into solid rock (i.e., US.BLA, US.MCWV, Table 1) whereas portable aftershock stations are often located in shallow temporary vaults in highly weathered and saturated soils (i.e., GS.ORRD, GS.SPRD, YC.IP01, YC.IP02, Table 1).

In the Q inversion, receiver terms are computed relative to a reference station. The reference station term is set to 1, and all remaining stations are then normalized relative to the reference station. Selection of a reference station is therefore important and several parameters should be considered. First, the reference station should have minimal to no site amplification. This requires that it be located on relatively well-consolidated hard rock in a permanent concrete vault, has low-background noise, and has well-known instrument response characteristics.

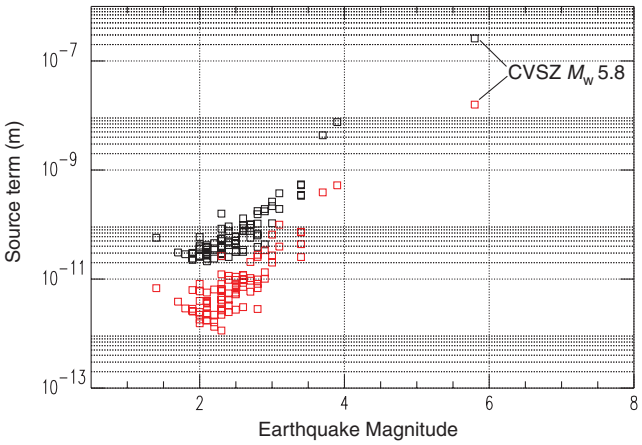

Figure 6. Eighty-eight 1.5 Hz (black squares) and 6 Hz (red squares) source terms determined from the average *Lg Q* inversion plotted versus earthquake magnitude are shown. A clear relationship exists with increasing source term and magnitude.

We employ a semi-quantitative approach in the selection of our reference station by computing horizontal-to-vertical spectral ratios (HVSR) to determine the range of possible amplifications and resonance frequencies in our station list. We apply a new approach that uses ambient noise microtremor spectral estimates for each seismic station from a spectral analysis system already established for routine quality-control monitoring at the USGS Albuquerque Seismological Laboratory (ASL) and National Earthquake Information Center (NEIC) (PQLX: McNamara and Boaz, 2010). In our analysis, the variation of spectral power is observed by computing instrument corrected power spectral density (PSD) probability density functions (PDFs) using the methods detailed in McNamara and Buland (2004). PSDs are combined into PDFs such that the distribution of spectral power over the given time period (28 August 2011–21 March 2012) is readily visualized and percentile statistics can be computed over a large population of PSDs (Fig. 7). In this study, HVSR site responses are formed as ratios of the PSD PDF distribution medians. To compute HVSR, we first convert spectra from dB to physical ground units of cm/s^2, calculate the geometric mean of the horizontal components, and then compute ratios for the horizontal components to the vertical. Figure 8 demonstrates the HVSR method described here for the USGS portable aftershock station, GS.SPFD (see map in Fig. 4, Table 1). PSDs computed using 11,940 hourly time segments overlapping by 50% from 28 August 2011 to 21 March 2012, are assembled in a PDF, for each component of motion, and the median of the distribution is computed (Fig. 7a–c). Horizontal component median spectra were then combined using an rms average, and individual station spectral ratios were calculated between the averaged PDF median horizontal component spectra and the vertical component PDF median (Fig. 8).

The HVSR results shown in Figure 8, for stations GS.SPFD and US.BLA, are an example of the strong variations in site response expected at seismic stations in the

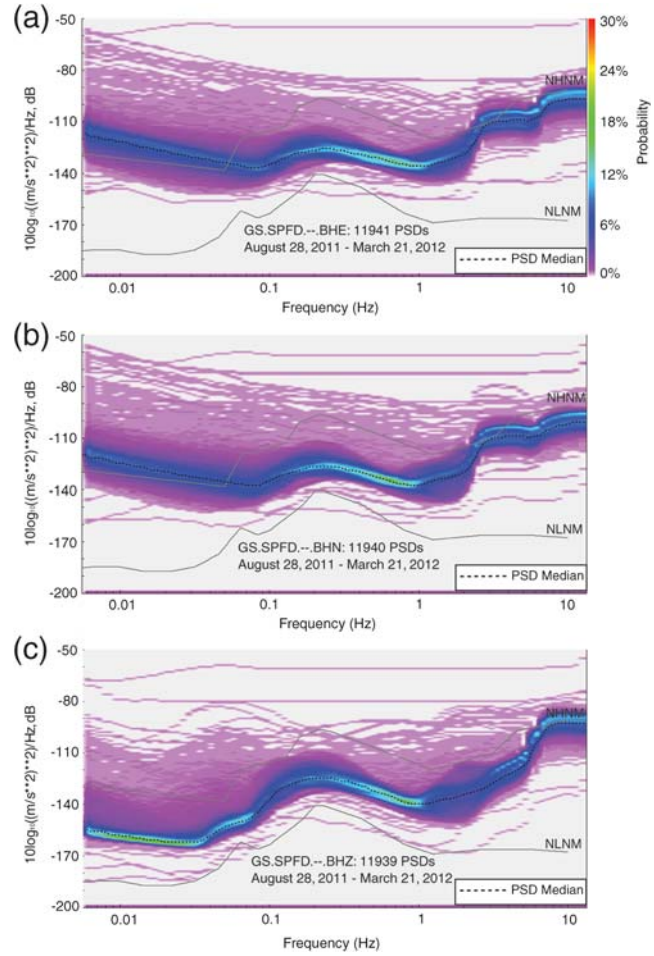

Figure 7. Power spectral density (PSD) probability density functions (PDFs) computed for three components of motion using portable aftershock station GS.SPFD are shown. PSD PDF medians are shown as black-dashed lines and used to form spectral ratios shown in Figure 8. (a) PDF formed from 11,941 PSDs recorded from 28 August 2011 to 21 March 2012 on channel GS.SPFD.—.BHE. (b) PDF formed from 11,940 PSDs recorded from 28 August 2011 to 21 March 2012 on channel GS.SPFD.—.BHN. (c) PDF formed from 11,939 PSDs recorded from 28 August 2011 to 21 March 2012 on channel GS.SPFD.—.BHZ. The new high- and low-noise models (gray lines NHNM, NLNM) are from Peterson (1993).

EUS. US.BLA is installed in a permanent sensor vault excavated into solid rock whereas aftershock sensors, such as GS.SPFD, were deployed in shallow vaults in loosely consolidated saprolite sediments and soils (Stolt *et al.*, 1991). As a result of the hard rock conditions, the mean HVSR estimate at US.BLA displays no significant ambient noise resonance frequency peaks (Fig. 8b). In contrast, a clear peak is observed at 3–4 Hz for the aftershock station GS.SPFD. For HVSR measured at additional permanent and aftershock stations, a broad range of resonance peaks are observed, ranging from 1 to 10 Hz, with some stations having additional multiple smaller peaks at higher frequencies (Odum *et al.*, 2012). Because the portable aftershock stations were deployed in shallow surface temporary vaults, they have local site amplifications

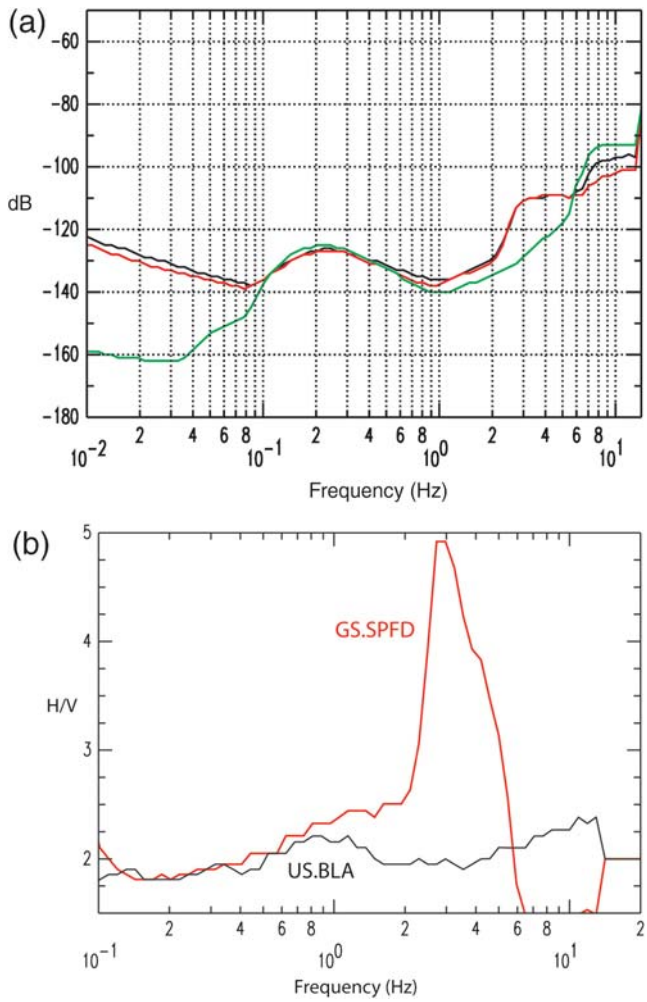

Figure 8. HVSR method using portable aftershock station GS.SPFD and Q inversion reference station US.BLA. (a) PSD PDF medians from Figure 7 are used to form spectral ratios to determine site response. GS.SPFD horizontal component PSD medians (red line, BHE, black line, BHN) are averaged and divided by the vertical (green line, BHZ). (b) GS.SPFD HVSR results display a clear resonance peak at 3 Hz with an amplification factor of 4 (red line) whereas the permanent ANSS rock-site US.BLA has none (black line).

that are much larger than our reference station, US.BLA. In addition, US.BLA recorded the mainshock and other regional aftershocks that occurred before the installation of the portable network. For these reasons, US.BLA was chosen as the reference station for all *Lg* Q inversions.

Site Geology and Receiver Terms

Much of the EUS, including Virginia, has unique geologic conditions that contribute to hazardous site response issues. First, along coastal zones, deep sediment stacks exist, resulting in the amplification of long-period motions. Second, at inland regions, high shear-wave velocity rock exists close to the surface, overlain by thin sediments, resulting in very high impedance contrasts and amplification at short periods (high frequencies). The geology of Virginia is marked by a wide variety of provinces from the coastal plains to the Appalachian plateau to the west. East of the Appalachian core, the Valley and Ridge province consists of elongated parallel ridges and valleys that are underlain by folded Paleozoic sedimentary rock. The Piedmont is the largest physiographic province in Virginia. It is bounded on the east by the Fall Zone, which separates the province from the Coastal Plain, and on the west by the mountains of the Blue Ridge province. The province is characterized by gently rolling topography, deeply weathered bedrock, and a relative paucity of solid rock outcrops. Rocks are strongly weathered in the Piedmont's humid climate and bedrock is generally buried under a thick (2–20 m) blanket of saprolite. Saprolite is the most prevalent soil parent material in the Piedmont and Blue Ridge Highlands regions of Virginia (Stolt *et al.*, 1991) and is generally formed in place as weathered material from the underlying bedrock. Saprolites are also common in other regions, such as Hong Kong, in which strong-motion site-response studies have determined the thin layers of saprolite overlying high-velocity bedrock can lead to significant site amplification (Pappin *et al.*, 2004; Koo *et al.*, 2005). For this reason there is a need to recognize that EUS sites have special conditions that require site-specific analysis.

Wave propagation theory suggests that ground-motion amplitude should depend on the density and shear-wave velocity of near-surface materials. Density has little variation with depth; so shear-wave velocity has become the most useful parameter to represent site conditions. Based on empirical studies (Borcherdt, 1994; Wills and Silva, 1998), the average shear-wave velocity in the upper 30 m (V_{S30}) has become the most common means of classifying site conditions and has been adopted in the National Earthquake Hazards Reduction Program (NEHRP) design provisions for new buildings (Martin, 1994). In general, higher V_{S30} values are associated with firm dense rock and lower levels of site amplification while lower V_{S30} values are associated with softer soils and high-site amplification.

V_{S30} is commonly computed by measuring the time it takes for shear waves to travel from 30 m depth to the surface using either active sources such as explosions or passive ambient noise microtremor sources (Odum *et al.*, 2010). Because this approach is limited to locations at which active measurements are undertaken, recent methods have sought to approximate V_{S30} globally using topographic slope (Allen and Wald, 2009). In this generalized approach high V_{S30} values are associated with the higher elevation spine of the Appalachian mountains in which soils and sediments are thin to nonexistent. In contrast, low V_{S30} values are found along the coastlines and in the flat regions of thicker sediments and soils, such as the Piedmont province (Hough, 2012).

Given the important nature and recent emphasis on understanding earthquake hazards in the EUS, V_{S30} was measured at several portable aftershock and permanent seismic stations in the Virginia and greater EUS region following the 2011 central Virginia earthquake (EPRI, 2012; Odum *et al.*,

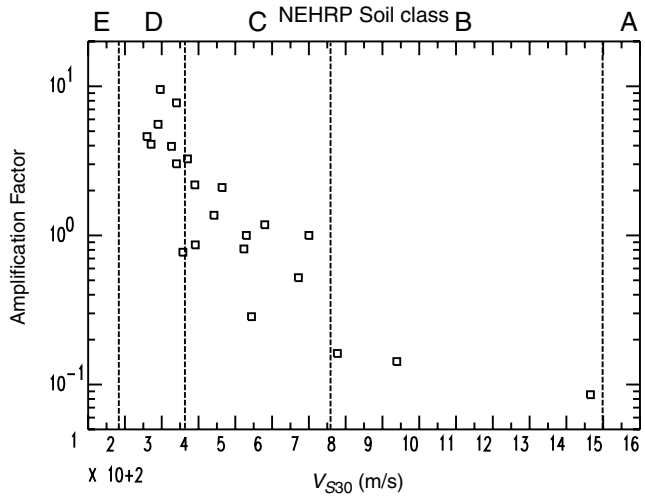

Figure 9. Average *Lg* Q inversion 3 Hz receiver terms versus measured V_{S30}. The Q inversion receiver term is expressed as an amplification factor relative to the reference station, US.BLA. NEHRP soil classes are defined by V_{S30} and shown above.

2012). Because of these studies, we have the opportunity to compare direct measurements of V_{S30} with the Q inversion receiver terms obtained in this study. V_{S30} measurements are not available for all 36 stations used in the average *Lg* Q inversion; however, V_{S30} measurements are available for many stations used in this study.

In Figure 9 we show the receiver terms determined in the average *Lg* Q inversion at 3 Hz, with 22 estimates of V_{S30} available from recent experiments conducted after the 2011 central Virginia earthquake. In general there is a good agreement between the receiver terms determined in this study and estimates of V_{S30} in which lower V_{S30} values correspond to less consolidated soils and higher amplification factors. In this study, we observe that larger receiver terms are associated with lower estimates of V_{S30}, suggesting that the receiver terms determined in the inversion reflect the amplifications of the permanent and portable stations relative to the reference station IU.BLA.

Q Inversion Uncertainty and Resolution

In order to understand the uncertainty associated with our methods, we examined the mean and standard deviation of Q_0 for all frequencies by resampling the original dataset using the delete-j Jackknife resampling technique (Erickson *et al.*, 2004; McNamara *et al.*, 2012). Figure 10a shows a histogram of the results obtained from 1000 different inversions of randomly selected Jackknife datasets using the average *Lg* amplitude dataset measured in the 2.0–4.0 Hz band (center frequency 3.0 Hz). We randomly removed 20% of the observations ($d = 221$) from the complete dataset ($n = 1108$) to create 1000 new Jackknife datasets, and then inverted each new reduced dataset to obtain 1000 Q values. The mean and standard deviation were calculated from this set of 1000 Q values to establish error estimates for the

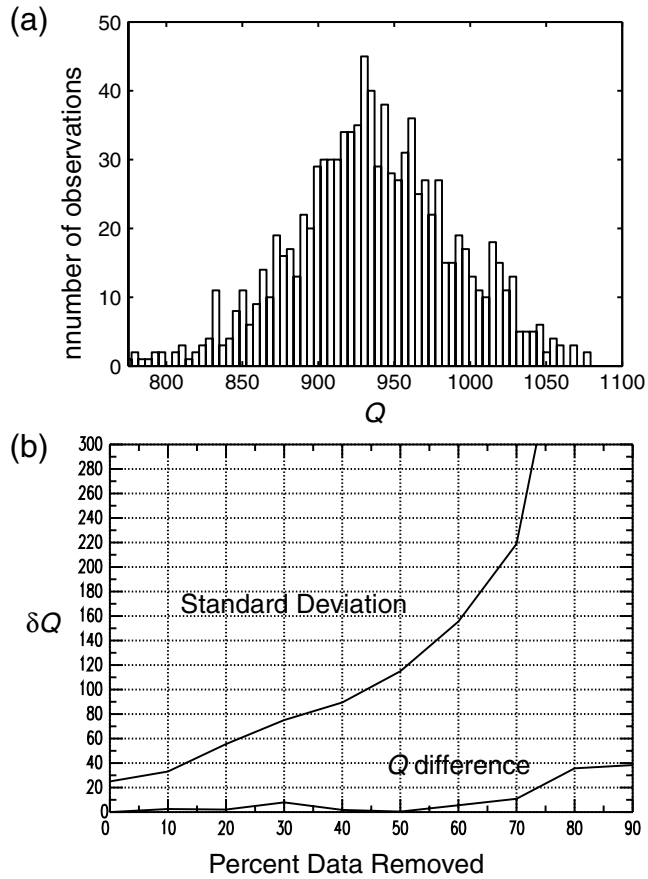

Figure 10. (a) Histogram of 1000 Jackknife datasets, with 20% removal, Q inversions using horizontal component *Lg* amplitudes at 3 Hz. In this example, the total number of observations $n = 1108$ and number of observations removed for each Jackknife inversion $d = 221$. Note the normal distribution of Q values. From 1000 randomly sampled datasets the average Jackknife Q has a value of 929.074 ± 55.53. (b) The difference between the average 3 Hz Q determined from 1000 Jackknife datasets and the 3 Hz Q inverted from the original complete dataset (black line) versus the percent of data removed. The upper line is the standard deviation of the Jackknifed Q result versus percent data removed from the original dataset.

region. In this example, Q_0 computed from the complete dataset is 931.14 (Fig. 10a). After 1000 randomly sampled datasets, with 20% reduction in the number of data points, the average Jackknife Q_0 value is 929.074 ± 55.53, a difference of only about 2 from the Q_0 determined using the complete dataset.

We also test the stability of our datasets by removing an increasing number of waveforms to determine at which point the inversion becomes unstable and Q_0 is no longer well resolved. In Figure 10b, note the standard deviation increases gradually until about 70% of the original data are removed. After 70% of the data are removed, standard deviation increases sharply even though the Q_0 difference remains reasonably low. The Q_0 difference gradually increases as an increasing percentage of data are removed. Note that the Q_0 difference is very low (<10) until 70% of the data are

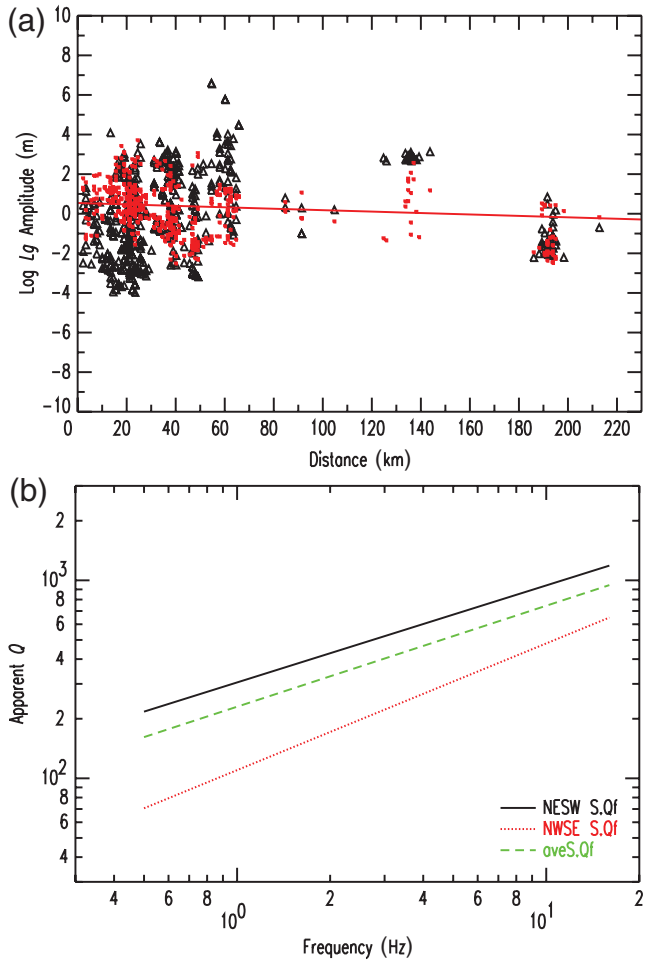

Figure 11. Examples of results from S-wave $Q(f)$ inversions. (a) Single frequency (1.5 Hz) Q fit (red line) 518 S-wave amplitudes <250 km with a NESW orientation, $Q = 372$. Raw amplitudes are shown as black triangles. The red squares are S-wave amplitudes with receiver and source terms removed. (b) CVSZ regional frequency dependent $Q(f)$ over five passbands for the average S-wave dataset ($Q(f) = 230(\pm 26)f^{0.51(\pm 0.11)}$), NESW S-wave paths ($Q(f) = 305(\pm 31)f^{0.49(\pm 0.050)}$), and NWSE S-wave paths ($Q(f) = 110(\pm 22)f^{0.64(\pm 0.055)}$).

removed and only increases to about 39 with as much as 90% of the data removed. This suggests that Q_0 can be determined with only 10% of our dataset (~100 observations), and adding more observations merely decreases uncertainty in the Q_0 estimate.

Average Local S-Wave $Q(f)$ Results

In addition to studying the attenuation characteristics of regional Lg, we determined $Q(f)$ using local (<250 km) distance horizontal component S-wave amplitudes. Similar to Lg procedures, S-wave amplitudes are measured in five frequency bands in order to determine the frequency dependence of $Q(f)$. S-wave amplitudes, corrected for the source (S_j) and receiver (G_i) terms are shown in Figure 11a for center frequency of 1.5 Hz and the straight lines represent

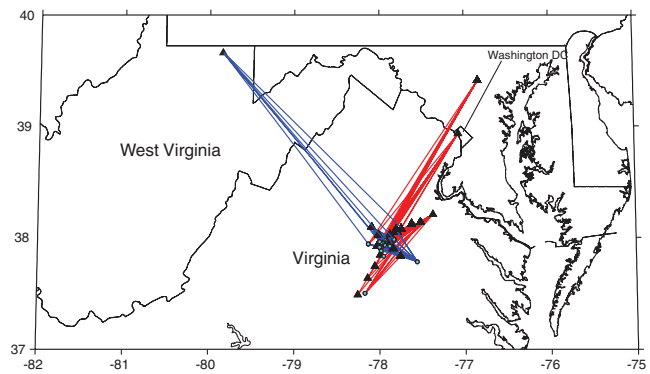

Figure 12. S-wave paths used in the $Q(f)$ inversions. Earthquakes are shown as blue circles and seismic stations are shown as black triangles. Red lines are 586 NESW S-wave paths parallel to strike of Appalachian mountains. Blue lines are 118 NWSE S-wave paths perpendicular to the regional tectonic fabric.

the best-fitting Q for the particular frequency band using equation (3). In each frequency band, the inversion procedure solves for an average Q using 970 high-quality S-wave amplitude observations, from 61 events, recorded at 25 stations, with a distance range of <250 km. We find an average S-wave $Q(f) = 230(\pm 26)f^{0.51(\pm 0.11)}$ using only horizontal component direct S waves with all path orientations (Fig. 11).

Azimuthal Variation of $Q(f)$

There is a large body of evidence suggesting that seismic energy in the EUS has a strong dependency on path. To test this hypothesis we divide the Lg- and S-wave propagation paths into groups roughly parallel and perpendicular to the tectonic fabric of the Appalachian mountains in the EUS (Figs. 4b,c and 12) and estimate Q for each set of paths separately. When compared with our regional averaged value of Lg $Q(f) = 751(\pm 39.0)f^{0.28(\pm 0.054)}$, we find higher Q_0 (by ~17%) and a similar frequency dependence (η) ($Q(f) = 877(\pm 41)f^{0.29(\pm 0.050)}$) using Lg paths roughly parallel to the strike of the Appalachian mountains and lower Q_0 (by ~15%) with a stronger frequency dependence (η) ($Q(f) = 636(\pm 32)f^{0.34(\pm 0.045)}$) using paths roughly perpendicular to the strike of EUS tectonic fabric.

S waves show a similar pattern. When compared with our average value of S wave $Q(f) = 230(\pm 26)f^{0.51(\pm 0.11)}$, we find higher Q_0 and a similar frequency dependence (η) ($Q(f) = 305(\pm 31)f^{0.49(\pm 0.050)}$) using S-wave paths roughly parallel to the strike of the Appalachian mountains and lower Q_0 with a stronger frequency dependence (η) ($Q(f) = 110(\pm 22)f^{0.64(\pm 0.055)}$) using paths roughly perpendicular to the strike of EUS tectonic fabric (Fig. 11b). These results indicate that both regional Lg waves and local S waves, propagating parallel to the fabric of the Appalachians, propagate more efficiently than paths propagating perpendicular to the Appalachians (Figs. 5c and 11b).

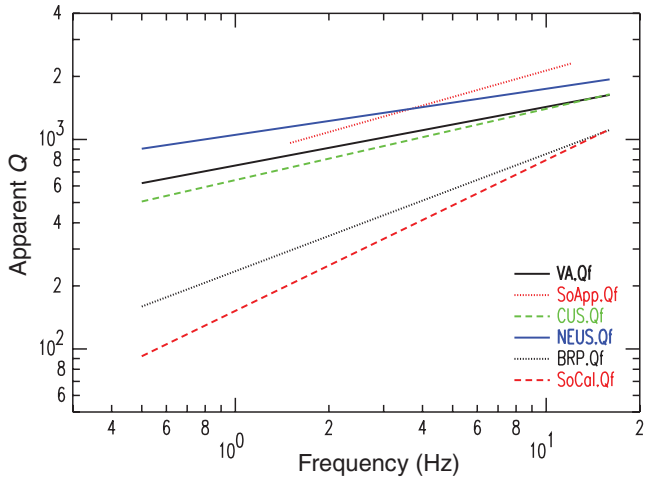

Figure 13. EUS average *Lg* $Q(f)$ results from this study (Virginia, $Q(f) = 751(\pm 39.0)f^{0.28(\pm 0.054)}$) compared with numerous regions that include: the northeastern United States (NEUS, $Q(f) = 1052f^{0.22}$, Benz *et al.*, 1997), central United States (CUS, $Q(f) = 640f^{0.34}$, Erickson *et al.*, 2004), Basin and Range province (BRP, $Q(f) = 235f^{0.56}$, Benz *et al.*, 1997), southern California (SoCal, $Q(f) = 152f^{0.72}$, Erickson *et al.*, 2004), and southern Appalachian mountains (SoApp, $Q(f) = 811f^{0.42}$, Chapman and Rogers, 1989).

Discussion

In this section we summarize results from our analysis in the CVSZ and surrounding region using data recorded during the aftershock deployment following the 2011 central Virginia earthquake. We present frequency-dependent Q results using local S waves (<250 km) and regional *Lg* waves and attempt to interpret them in a tectonic and geological hazard context.

High Q in the Eastern United States

Ground shaking associated with the 2011 central Virginia earthquake was felt over a larger region than any previous instrumentally recorded earthquake in the EUS (Horton and Williams, 2012; Hough, 2012). This is consistent with numerous studies that demonstrate efficient energy propagation through crystalline bedrock that underlies much of the eastern margin of the United States (Jones *et al.*, 1977). Results from this study are consistent with the now common observation of high Q values in the EUS relative to the WUS (Frankel *et al.*, 1990; Frankel *et al.*, 1996; Atkinson, 2004). We compare the average *Lg* $Q(f)$ results from this study with previous results from other regions, including the northeastern United States (NEUS, Benz *et al.*, 1997), CUS (Erickson *et al.*, 2004), Basin and Range province (BRP, Benz *et al.*, 1997), southern California (SoCal, Erickson *et al.*, 2004), and the southern Appalachians (Fig. 13) (Chapman and Rogers, 1989). Not surprisingly, the regional *Lg* $Q(f)$ results from this study are most similar to the CUS and southern Appalachian results (Chapman and Rogers, 1989; Chapman *et al.*, 2003; Erickson *et al.*, 2004) and thus are consistent with values estimated previously for tectonically stable regions.

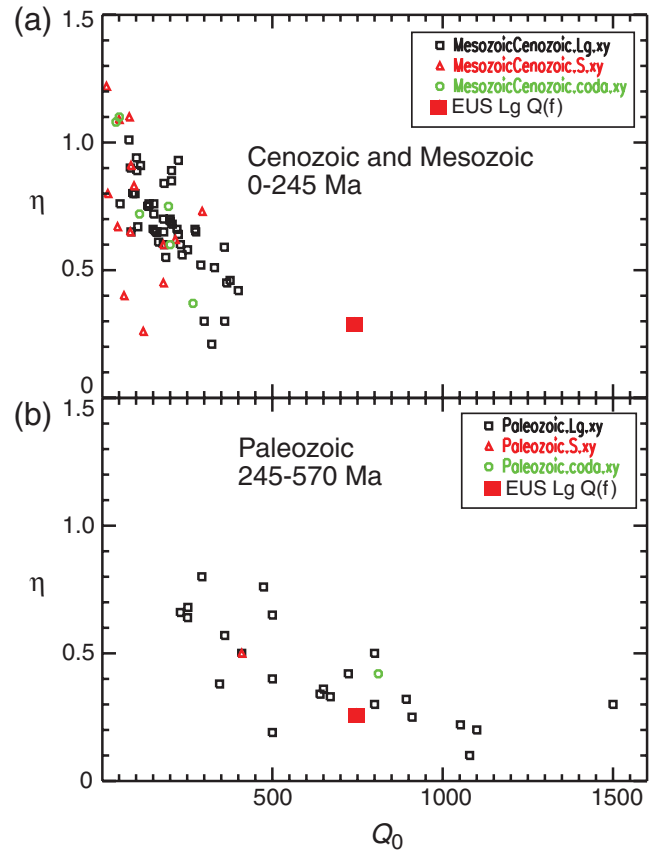

Figure 14. EUS $Q(f)$ results from this study compared with attenuation parameters (Q_0 and η) from numerous studies in two different thermotectonic ages. We include results from this study (red square) in each panel to demonstrate the affinity of EUS region. (a) Cenozoic and Mesozoic, (b) Paleozoic. The method and seismic wave used is denoted by color and symbol shape. Black squares are Q study results that used regional *Lg*, red triangles used local S waves, and green circles are Q values determined using coda decay methods.

We extend this comparison with other tectonic environments by determining the connection between attenuation parameters and thermotectonic age for a number of published studies. thermotectonic age is defined as the age of the last thermotectonic event and refers to the age in which the last major event to influence the crustal structure took place. thermotectonic age was determined by locating each of the attenuation study regions on the high-resolution USGS thermotectonic map following methods described in McNamara *et al.* (2011). In Figure 14, we plot the attenuation parameters (Q_0 and η) for numerous studies determined in regions with crust of two different thermotectonic ages. The most striking observation from Figure 14 is that with increasing thermotectonic age, the crust frequency dependence (η) decreases while Q increases. Mitchell and Cong (1998) observed a similar relationship by comparing Q determined from coda methods in the stable continental regions of Africa and

North America. McNamara *et al.* (2011) extended the observation to include regional Q results obtained using different methods and from additional tectonic environments. In this study we also observe that attenuation parameters obtained from this study for the EUS are well outside of the distribution of younger (0–245 Ma) crust and more consistent with older Paleozoic age crust (245–570 Ma) associated with the Appalachian mountains.

Additional evidence in support of high Q in the EUS comes from the distribution of rock falls. Jibson and Harp (2012) mapped the occurrence of rockfalls after the central Virginia earthquake mainshock to determine distance limits that could be compared with those from other documented earthquakes. Previous studies using a global set of earthquakes predicted an average maximum epicentral distance of about 60 km for an M_w 5.8 earthquake (Keefer, 1984). The maximum distance limit for the 2011 central Virginia earthquake was 245 km, the largest exceedance of the historical limit ever observed, by nearly a factor of 4. Similarly, the previous maximum area affected by landslides for an M_w 5.8 earthquake was 1500 km^2 while the area affected by landslides in the 2011 central Virginia earthquake was 33, 400 km^2. While the distribution of observed rockfalls depends on several factors such as the time to the last large event, regional topography, and climate, Jibson and Harp (2012) note that their results are consistent with strong motions generated by the 2011 central Virginia earthquake. The large exceedance limit and maximum rockfall distance observations are also consistent with our high *Lg* Q results and provide physical evidence that attenuation of shaking for EUS earthquakes is significantly lower (higher Q) than for plate-boundary earthquakes.

Preferential Orientation of Q

There is a large body of existing evidence now suggesting that seismic energy in the EUS displays a clear azimuthal preference, with more efficient propagation occurring along the strike of the tectonic fabric associated with the Appalachian mountains. Previous observations include: (1) the distribution of felt reports from the recent 2011 M_w 5.8 central Virginia earthquake (Hough, 2012); (2) the distribution of intensity from historical EUS earthquakes (1969 West Virginia earthquake, Bollinger and Hopper [1970]; 1897 Giles County Virginia and 2003 CVSZ earthquakes, Tarr and Wheeler [2006]); (3) anisotropic strong-motion and *Lg*-phase propagation efficiency (e.g., Jones *et al.*, 1977; Hough *et al.*, 1989); and (4) the asymmetrical distribution of rockfalls and landslides (Jibson and Harp, 2012). In the Jibson and Harp (2012) study, landslide and rockfall distance limits are shown to have an asymmetrical/elongated pattern, with a long axis parallel to the regional structural trend of the Appalachian mountains. They suggest that their observation is consistent with the mainshock intensity distribution and is related to the regional geologic structure (Hough, 2012).

Several mechanisms could explain the observed preferred shaking orientation including site effects, source directivity, and preferred propagation path due to properties of the crust. In an effort to isolate site effects from propagation path and source effects, Hough (2012) demonstrates that site effects from the 2011 central Virginia earthquake have a significant effect on shaking intensity and show a good correlation with V_{S30} values determined from topographic slope methods (Allen and Wald, 2009), but do not show a distribution consistent with preferred propagation orientation. Hough (2012) therefore concludes that the effects of preferred propagation direction and source directivity influence shaking intensities with roughly equal contributions. Site terms from this study are consistent with this general conclusion in that they display no azimuth-dependent distribution and correlate roughly with V_{S30} values and NEHRP soil class (Fig. 9).

In an effort to isolate the effects of source directivity and preferred path orientation, we removed the M_w 5.8 CVSZ mainshock from our *Lg*-amplitude dataset and ran the Q inversion using only small-magnitude aftershocks. $Q(f)$ results for all three path groups, determined using only aftershocks, were well within the standard deviation of the original complete datasets. This is demonstrated in Figure 5c, where the Q inversion was performed using only aftershocks with paths in the NESW direction. In this case, the Q result was virtually unchanged. This observation strongly suggests that mainshock source directivity has little to no influence on the azimuthally dependent Q results and we conclude that preferred propagation path due to properties of the crust is the significant mechanism for our Q estimates and observations of preferred intensity distribution (Hough, 2012).

Lg Q is a function of both intrinsic material properties and scattering effects along the propagation path. Several studies have attempted to isolate the effects of scattering and intrinsic rock properties on the attenuation $(1/Q)$ of seismic energy. In a study comparing results from Hawaii and California, Mayeda *et al.* (1992) demonstrate that scattering Q is more strongly frequency dependent than intrinsic Q. Our results show lower Q_0 with a much stronger frequency dependence (η) using paths roughly perpendicular to the strike of EUS tectonic fabric compared with the regional average and using only paths parallel to the Appalachian mountains (Fig. 4). This observation is consistent with conclusions reached by Mayeda *et al.* (1992) and suggests that scattering has a stronger influence on Q for paths crossing the Appalachians mountains relative to paths parallel to the mountain chain. Intrinsic rock properties are not expected to change parallel to the strike of the tectonic fabric because geologic units, contacts, and faults should be roughly continuous. Based on these observations, we conclude that paths perpendicular to tectonic strike experience a higher degree of scattering along faults and contacts associated with the fabric of the Appalachian mountains.

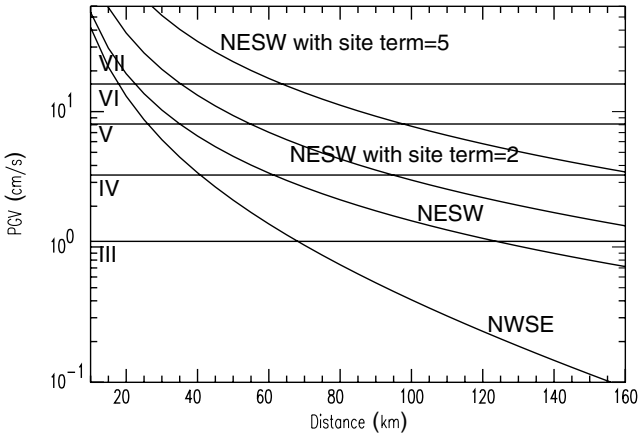

Figure 15. PGV versus distance models for two different *S*-wave Q functions with different path orientations (NWSE, NESW). Results assuming two NESW models that include site amplifications of a factor of 2 and 5 are also shown.

The Relationship between Intensity, Q, Source Directivity, and Site Amplification

Hough (2012) observes that the distribution of felt intensity from the 2011 central Virginia earthquake is asymmetric with higher intensities having an NESW-directed preferred orientation for several hundred kilometers from the CVSZ. In an attempt to explain this observation, Hough (2012) suggests that the effects of preferred propagation direction and source directivity together serve to influence shaking intensities by as much as 1.0–1.2 Mercalli intensity units, with roughly comparable contributions from each effect. Hough (2012) also suggests that in order to explain the occurrences of strong shaking in the Washington, D.C. area, significant site amplification, due to soft soils, is required in addition to Q variation and directivity effects.

Previously, we demonstrated that mainshock source directivity likely has little effect on the distribution of the azimuthal dependence of Q, by removing mainshock amplitude data from Q inversion datasets. Q estimates are virtually unchanged when the mainshock is removed (Fig. 5c) suggesting that source directivity has no significant effect. In an effort to further understand the relative contributions of preferred propagation direction, source directivity, and site amplification, we model local and regional peak *S*-wave amplitudes after Brune (1970, 1971) to test the sensitivity of shaking intensity to the various Q models determined in this study. Because we are modeling peak *S*-wave amplitudes that occur at the source corner frequency, we suggest that *S*-wave amplitudes determined using this approach should be a close approximation of peak ground velocity (PGV). PGV can then be related directly to instrumental intensity (II) using empirical relationships presented by Wald *et al.* (1999). In this analysis, we estimate II for various Q models from this study to determine if Q alone can account for the range of shaking intensities observed in Hough (2012). The distance ranges of most interest in this analysis, epicenter to Washington, D.C. (100–160 km), correspond to the *S*-wave distances (Frankel *et al.*, 1990; Atkinson, 2004), therefore assumptions of Q that we test are taken from the *S*-wave inversion results described in this study.

After Brune (1970, 1971) shear-wave amplitude (As) is modeled as

$$As = \frac{M_o}{4\mu\beta} \times \frac{f_c}{\Delta}, \tag{6}$$

in which M_o is the *W*-phase moment (5.7×10^{24} dyn·cm), μ is the rigidity (30 GPa), β is shear-wave velocity (3.5 km/s), f_c is the source corner frequency, Δ is the source–receiver distance.

To determine As, we must first estimate source corner frequency after

$$f_c = \frac{2.21\beta}{2\pi r}, \tag{7}$$

in which r is the fault dimension.

Fault dimension is related to moment (M_o) after Brune (1970, 1971)

$$M_o = 2.29\sigma r^3 \quad \text{in dyn·cm}, \tag{8}$$

in which M_o is *W*-phase moment (5.7×10^{24} dyn·cm) (McNamara *et al.*, 2014), σ is the source static stress drop, 50 MPa (Ellsworth *et al.*, 2011).

Finally we apply the appropriate Q and geometric spreading terms (γ) to the Brune *S*-wave amplitude estimate (As) from equation (6) to determine the corrected *S*-wave amplitude (Ac).

$$Ac = \frac{As}{\Delta^\gamma} \times e^{\frac{-\pi f m \Delta}{Q\beta}}, \tag{9}$$

in which geometrical spreading (γ) is a function of source–receiver distance (Δ) in the EUS (Atkinson, 2004). For simplicity we assume a single geometrical spreading of $\gamma = 1.0$ because the distance ranges of most interest in this analysis, epicenter to Washington, D.C. (100–160 km), correspond to the *S*-wave distances. Appropriate assumptions of Q, tested in this analysis, are then taken from the *S*-wave inversions determined using ray paths <250 km in length.

Figure 15 is a plot of PGV assuming two different local *S*-wave $Q(f)$ functions determined in this study for paths orientated in NESW and NWSE directions (Figs. 11 and 12). Paths with NESW orientation have higher *S*-wave $Q(f)$ functions ($Q(f) = 305(\pm 31)f^{0.49(\pm 0.050)}$) than paths orientated in an NWSE direction ($Q(f) = 110(\pm 22)f^{0.64(\pm 0.055)}$). Also shown are the boundaries between instrumental intensity levels III–IV and IV–V from Wald *et al.* (1999). At specific distances, similar to the path from the CVSZ and Washington, D.C. area (110 km), the two Q models alone can account for nearly a full intensity unit. Because the range of intensity intervals is broad, it is difficult to specifically quantify and we must use some caution. For example, modeling a full-intensity-unit variation is strongly dependent on the distance.

We also show PGV models with site amplifications of a factor of 2 and 5 applied. At 120 km distances, the two different Q models produced roughly the same shaking intensity (III). When a station amplification of 2 is applied, shaking intensity reaches IV, and at station amplification of 5, intensity levels reach to as high as V. In order to account for the variability in shaking intensity in the Washington, D.C. area, we suggest that Q variations alone do not account for 100% of the intensity variations (1–1.2) (Hough, 2012) and that to match observed intensities of V in the Washington, D.C. area, significant site amplification is required.

Conclusions

In this study, we determine attenuation parameters (Q_0 and η) for the CVSZ and the surrounding EUS region. The most significant result from this study is that Q in the EUS is high at both local and regional distances, with a strong preferential orientation. We find that average attenuation $Q(f)$ results are consistent with previous studies in the region and studies in similar environments. We also observe an azimuthal dependence of $Q(f)$ that is consistent with the structural trend of the Appalachian mountains and explains a significant portion of the northeast-trending felt distribution as observed in the USGS "Did You Feel It" website.

We demonstrate that the contribution of azimuthally dependent Q is sufficient to explain distribution of felt intensity reported by Hough (2012) on a broad regional scale; however, additional factors such as site amplification are required in order to explain specific intensity observations in regions such as Washington, D.C. and coastal areas of the northeast. Additional work is required to compute unmodeled effects of source directivity on observed shaking intensities based on this study; source directivity of the mainshock has little effect on our estimates of Q.

We theorize that scattering along faults associated with the tectonic fabric of the Appalachian mountains is the primary cause of the observed azimuthal dependence of Q. This theory should be further tested in modeling approaches and/or possibly examining the differences in other empirical Q methods, such as coda Q, as a function of path azimuth. With the arrival of the EarthScope Transportable Array, future work should include high-resolution $Q(f)$ tomography inversion (Pasyanos *et al.*, 2009) that includes a term to solve for azimuthal anisotropy similar to methods used to simultaneously invert for lateral velocity variations and anisotropy (Hearn, 1996).

Attenuation parameters from this study contribute to a global database of tectonic environment and region-specific $Q(f)$ that is important to simulate strong ground shaking for hazard mitigation planning. Results from this and similar studies in the EUS are rare and important for the improvement of probabilistic assessments of seismic hazard, such as the USGS national seismic-hazard maps that are used for seismic provisions in building codes.

Data and Resources

The waveforms used in this study include both horizontal and vertical components of motion from crustal earthquakes recorded at local and regional distances. Events analyzed include the devastating M_w 5.8 central Virginia earthquake and the rich sequence of aftershocks (Fig. 1; Table 2). All waveforms were visually inspected and restricted to well-recorded ($M \geq 1.5$), crustal earthquakes (depth ≤ 20 km). Data used in this study were digitally recorded at regional broadband stations operated by the USGS ANSS, GSN, EarthScope Transportable Array, and U.S. regional seismic networks. In addition, 47 portable stations were deployed shortly after the 2011 central Virginia earthquake (Fig. 1, Table 2). Earthquake locations and magnitudes used in this study were obtained from USGS PDE. All waveform data, from both portable and permanent seismic stations, used in this study are archived and available for download from the IRIS DMC. Analysis and mapping software used includes Seismic Analysis Code (SAC; Goldstein *et al.*, 2003; Goldstein and Snoke, 2005), Generic Mapping Tools (GMT; Wessel and Smith, 1991, 2004) and MATLAB.

Additional data and resources were obtained from the following websites: spectral ratios were computed using the software package PQLX (McNamara and Boaz, 2010) and can be found at http://earthquake.usgs.gov/research/software/pqlx.php (last accessed June 2013). Strong-motion models GMPEs shown in Figure 1 were calculated using the random vibration theory implemented by the SMSIM program (Boore, 2000). Tectonic ages of the numerous *Lg* study areas shown in Figure 14 were determined from the USGS thermotectonic map, http://earthquake.usgs.gov/research/structure/crust/maps.php (last accessed March 2012). PGA values from the M_w 5.8 central Virginia earthquake, plotted in Figure 1, were obtained from the USGS Shakemap system instrumental intensity website at http://earthquake.usgs.gov/earthquakes/shakemap/global/shake/082311a (last accessed November 2012). We also used data from the Earthscope Transportable array (USArray, http://www.usarray.org/researchers/obs/transportable; last accessed December 2012).

Acknowledgments

The authors greatly appreciate the rapid response and hard work of the aftershock deployment field crew. The crew included Steve Horton, Mitch Withers, Won-Young Kim, Bob Herrmann, Patrick Bastion, Noel Barstow, and additional staff from the USGS and IRIS PASSCAL Field support for the IRIS PASSCAL stations was provided by NSF Grant EAR1148357 to Lehigh University. We would also like to thank staff at the USGS NEIC (A. Leeds, J. Allen, M. Meremonte), IRIS PASSCAL, UNAVCO, and station hosts in Louisa County, Virginia, for material and logistical support. The authors would like to thank M. Petersen, A. Frankel, R. Williams, A. Shah, and W. Horton for helpful discussions on the relationship between attenuation and earthquake hazard in the EUS. Thoughtful comments were provided by S. Hough, S. Hartzell, J. McCarthy, Tom Hearn, and one anonymous BSSA reviewer. Any use of trade, product, or firm names is for descriptive purposes only and does not imply endorsement by the U.S. Government.

References

Aki, K. (1980). Scattering and attenuation of shear waves in the lithosphere, *J. Geophys. Res.* **85,** 6496–6504.

Allen, T. I., and D. J. Wald (2009). On the use of high-resolution topographic data as a proxy for seismic site conditions (V_{S30}), *Bull. Seismol. Soc. Am.* **99,** no. 2A, 935–943.

Aster, R. C., B. Borchers, and C. H. Thurber (2005). *Parameter Estimation and Inverse Problems*, Elsevier Academic Press, London, 301 pp.

Atkinson, G. M. (2004). Empirical attenuation of ground motion spectral amplitudes in southeastern Canada and the northeastern United States, *Bull. Seismol. Soc. Am.* **94,** 1079–1095.

Atkinson, G. M., and D. M. Boore (1995). New ground motion relations for eastern North America, *Bull. Seismol. Soc. Am.* **85,** 1730.

Atkinson, G. M., and R. Mereu (1992). The shape of ground motion attenuation curves in southeastern Canada, *Bull. Seismol. Soc. Am.* **82,** 2014–2031.

Benz, H., A. Frankel, and D. M. Boore (1997). Regional *Lg* attenuation for the continental United States, *Bull. Seismol. Soc. Am.* **87,** 606–619.

Bollinger, G. A., and M. G. Hopper (1970). The Elgood, West Virginia earthquake of November 20, 1969, *Earthq. Notes* **41,** 19–30.

Boore, D. M. (1983). Stochastic simulation of high-frequency ground motions based on seismological models of the radiated spectra, *Bull. Seismol. Soc. Am.* **73,** 1865–1894.

Boore, D. M. (2000). SMSIM-Fortran programs for simulating ground motions from earthquakes, *U.S. Geol. Surv. Open-File Rept. 00-509*, 56 pp.

Borcherdt, R. D. (1994). Estimates of site-dependent response spectra for design morphology and justification, *Earthq. Spectra* **10,** 617–653.

Brune, J. (1970). Tectonic stress and the spectra of seismic shear waves from earthquakes, *J. Geophys. Res.* **75,** 4997–5009.

Brune, J. (1971). Correction, *J. Geophys. Res.* **76,** 5002.

Chapman, M. C. (2013). On the rupture process of the 23 August 2011 Virginia earthquake, *Bull. Seismol. Soc. Am.* **103,** no. 2A, 613–628.

Chapman, M. C., and M. J. B. Rogers (1989). Coda Q in the southern Appalachians, *Geophys. Res. Lett.* **16,** no. 6, 531–534, doi: 10.1029/GL016i006p00531.

Chapman, M. C., P. Talwani, and R. C. Cannon (2003). Ground motion attenuation in the Atlantic Coastal Plain near Charleston, South Carolina, *Bull. Seismol. Soc. Am.* **93,** 998–1011.

Chavez, D., and K. Priestly (1986). Measurement of frequency dependent *Lg* attenuation in the Great Basin, *Geophys. Res. Lett.* **13,** 551–554.

Earthquake Engineering Research Institute (EERI) Special Earthquake Report (2011). Learning from earthquakes: The M_w 5.8 Virginia earthquake of August 23, 2011, 13 pp., http://www.eqclearinghouse.org/2011-08-23-virginia/files/2011/12/EERI-GEER-DRC-Virginia-eq-report.pdf (last accessed September 2013).

Electric Power Research Institute (EPRI) (2012). Ground-motion model (GMM) review project, 2012 Shear Wave Velocity Measurements at Seismic Recording Stations, EP-P43952/C19088.

Ellsworth, W. L., K. Imanishi, J. H. Luetgert, J. Kruger, and J. Hamilton (2011). The M_w 5.8 Virginia earthquake of August 23, 2011 and its aftershocks: A shallow high stress drop event, *American Geophysical Union, 2011 Fall Meeting*, San Francisco, California, S14B-05.

Erickson, D., D. E. McNamara, and H. M. Benz (2004). Frequency dependent *Lg* Q within the continental United States, *Bull. Seismol. Soc. Am.* **94,** no. 5, 1630–1643.

Frankel, A. (1991). Mechanisms of seismic attenuation in the crust: Scattering and anelasticity in New York State, South Africa and, southern California, *J. Geophys. Res.* **96,** 6269–6289.

Frankel, A., A. McGarr, J. Bicknell, J. Mori, L. Seeber, and E. Cranswick (1990). Attenuation of high-frequency shear waves in the crust: measurements from New York state, South Africa and, southern California, *J. Geophys. Res.* **95,** 17,441–17,457.

Frankel, A., C. Mueller, T. Barnhard, D. Perkins, E. Leyendecker, N. Dickman, S. Hanson, and M. Hopper (1996). National seismic-hazard maps: Documentation June 1996, *U.S. Geol. Surv. Open-File Rept. 96-532*, 110 pp.

Garcia, D., S. Krishna Singh, M. Herraiz, J. Pacheco, and M. Ordaz (2004). Inslab earthquakes of central Mexico: Q, source spectra, and stress drop, *Bull. Seismol. Soc. Am.* **94,** no. 3, 789–802.

Goldstein, P., and A. Snoke (2005). SAC availability for the IRIS community, DMS Electronic Newsletter **7,** no. 1, 63 pp.

Goldstein, P., D. Dodge, M. Firpo, and L. Minner (2003). SAC2000: Signal processing and analysis tools for seismologists and engineers, Invited contribution to *The IASPEI International Handbook of Earthquake and Engineering Seismology*, W. H. K. Lee, H. Kanamori, P. C. Jennings, and C. Kisslinger (Editors), Academic Press, London.

Gregersen, S. (1984). *Lg*-wave propagation and crustal structure differences near Denmark and the North Sea, *Geophys. J. Roy. Astron. Soc.* **79,** 217–234.

Gutenberg, B. (1955). Channel waves in the Earth's crust, *Geophysics* **20,** 283–294.

Hearn, T. M. (1996). Anisotropic Pn tomography in the western United States, *J. Geophys. Res.* **101,** no. B4, 8403–8414.

Horton, J. W., and R. A. Williams (2012). The 2011 Virginia earthquake: What are scientists learning? *Eos Trans. AGU* **93,** 33.

Hough, S. E. (2012). Initial assessment of the intensity distribution of the 2011 M_w 5.8 Mineral, Virginia earthquake, *Seismol. Res. Lett.* **83,** 649–657.

Hough, S. E., K. Jacob, and P. Friberg (1989). The 11/25/88, $M = 6$ Saguenay Earthquake near Chicoutimi, Quebec: Evidence for anisotropic wave propagation in northeastern North America, *Geophys. Res. Lett.* **16,** 645–648.

Isacks, B. L., and C. Stephens (1975). Conversion of *Sn* to *Lg* at a continental margin, *Bull. Seismol. Soc. Am.* **65,** 235–244.

Jibson, R. W., and E. L. Harp (2012). Extraordinary distance limits of landslides triggered by the 2011 Mineral, Virginia earthquake, *Bull. Seismol. Soc. Am.* **102,** no. **6**, 2368–2377.

Jones, F. B., L. T. Long, and J. H. McKee (1977). Study of the attenuation and azimuthal distribution of seismic-wave propagation in the southeastern United States, *Bull. Seismol. Soc. Am.* **67,** 1503–1513.

Joshi, A., and S. Midorikawa (2004). A simplified method for simulation of strong ground motion using rupture model of the earthquake source, *J. Seismol.* **8,** 467–484.

Keefer, D. K. (1984). Landslides caused by earthquakes, *Geol. Soc. Am. Bull.* **95,** 406–421.

Kennett, B. (1986). *Lg* waves and structural boundaries, *Bull. Seismol. Soc. Am.* **76,** 1133–1141.

Kim, W.-Y., and M. C. Chapman (2005). The 9 December 2003, central Virginia, earthquake Sequence: A compound earthquake in the central Virginia seismic zone, *Bull. Seismol. Soc. Am.* **95,** 2428–2445.

Knopoff, L. (1964). Q, *Rev. Geophys.* **2,** 625–660.

Knopoff, L., F. Schwab, and E. Kaussel (1973). Interpretation of *Lg*, *Geophys. J. Roy. Astron. Soc.* **33,** 389–404.

Koo, R., V. Kong, and M. Free (2005). Seismic hazard assessment and site response evaluation in Hong Kong, in *Proc. of the SECED Young Engineers Conference*, University of Bath, Bath, United Kingdom, 21–22 March 2005.

Martin, G. R. (Editor) (1994). *Proc. NCEER/SEAOC/BSSC Workshop on Site Response During Earthquakes and Seismic Code Provisions*, University of Southern California, 18–20 November 1992.

Mayeda, K., S. Koyanagi, M. Hoshiba, K. Aki, and Y. Zeng (1992). A comparative study of scattering, intrinsic, and coda Q^{-1} for Hawaii, Ling Valley, and Central California between 1.5 and 15.0 Hz, *J. Geophys. Res.* **97,** no. B5, 6643–6659, doi: 10.1029/91JB03094.

McNamara, D. E. (2000). Frequency dependent *Lg* attenuation in south-central Alaska, *Geophys. Res. Lett.* **27,** 3949–3952.

McNamara, D. E., and R. I. Boaz (2010). PQLX: A seismic data quality control system description, applications and users manual, *U.S. Geol. Surv. Open-File Rept. 2010-1292*, 41 pp.

McNamara, D. E., and R. Buland (2004). Ambient noise levels in the continental United States, *Bull. Seismol. Soc. Am.* **94,** 1517–1527.

McNamara, D. E., and W. Walter (2001). Mapping crustal heterogeneity using *Lg* propagation efficiency throughout the Middle East, Mediter-

ranean, southern Europe and northern Africa, *Pure Appl. Geophys.* **158,** 1165–1188.

McNamara, D. E., H. Benz, L. S. Gee, and A. D. Frankel (2011). A global survey of frequency dependent seismic attenuation, *American Geophysical Union, Fall Meeting 2011*, San Francisco, California, 5–9 December 2011, Abstract #S51C–2234

McNamara, D. E., H. Benz, R. Herrmann, E. A. Bergman, P. Earle, A. Meltzer, M. Withers, and M. Chapman (2014). The M_w 5.8 central Virginia earthquake of August 2011 and aftershock sequence: Constraints on earthquake source parameters and fault geometry, *Bull. Seismol. Soc. Am.* **104,** doi: 10.1785/0120130058.

McNamara, D. E., M. Meremonte, J. Z. Maharrey, S-L. Mildore, J. R. Altidore, D. Anglade, S. E. Hough, D. Given, H. Benz, L. Gee, and A. Frankel (2012). Frequency-dependent seismic attenuation within the Hispaniola Island region of the Caribbean Sea, *Bull. Seismol. Soc. Am.* **102,** no. 2, doi: 10.1785/0120110137.

McNamara, D. E., T. J. Owens, and W. R. Walter (1996). Propagation characteristics of *Lg* across the Tibetan Plateau, *Bull. Seismol. Soc. Am.* **86,** 457–469.

Menke, W. (1980). *Geophysical Data Analysis: Discrete Inverse Theory*, Academic Press, Inc., San Diego, California.

Mitchell, B. J. (1981). Regional variation and frequency dependence of $Q\beta$ in the crust of the United States, *Bull. Seismol. Soc. Am.* **71,** 1531–1538.

Mitchell, B. J., and L. Cong (1998). *Lg* coda *Q* and its relation to the structure and evolution of continents: A global perspective, *Pure Appl. Geophys.* **153,** 655–663.

Morozov, I. B. (2008). Geometrical attenuation, frequency dependence of *Q*, and the absorption band problem, *Geophys. J. Int.* **175,** 239–252.

Morozov, I. B. (2011). Mechanisms of geometrical attenuation, *Ann. Geophys.* **54,** 3.

Odum, J. K., W. J. Stephenson, D. E. McNamara, and S. J. Angster (2012). Preliminary passive and active source V_{S30} results at 18 portable seismograph stations deployed to study the M_w 5.8 Mineral, VA, 23 August 2011 earthquake, *Geol. Soc. Am. Abstracts with Programs*, **44,** no. 7, 592.

Odum, J. K., W. J. Stephenson, and R. A. Williams (2010). Predicted and observed spectral response from co-located shallow, active and passive source V_S data at five ANSS sites, Illinois and Indiana, USA, *Seismol. Res. Lett.* **81,** no. **6**, 955–964.

Oliver, J., and M. Ewing (1957). Higher mode surface waves and their bearing on the Earth's mantle, *Bull. Seismol. Soc. Am.* **47,** 187–204.

Ottemoller, L. (2002). *Lg* wave *Q* tomography in central America, *Geophys. J. Int.* **150,** 295–302.

Pappin, J. W., M. W. Free, J. Bird, and R. Koo (2004). Evaluation of site effects in a moderate seismicity region, Hong Kong, in *13th World Conference on Earthquake Engineering*, Vancouver, B.C., Canada, August, 2004.

Pasyanos, M. E. (2011). A case for the use of 3D attenuation models in ground-motion and seismic-hazard assessment, *Bull. Seismol. Soc. Am.* **101,** no. 4, 1965–1970, doi: 10.1785/0120110004.

Pasyanos, M. E, W. R. Walter, and E. M. Matzel (2009). A simultaneous multiphase approach to determine *P*-wave and *S*-wave attenuation of the crust and upper mantle, *Bull. Seismol. Soc. Am.* **99,** 3314–3325.

Peterson, J. (1993). Observation and modeling of seismic background noise, *U.S. Geol. Surv. Tech. Rept. 93-322*.

Press, F., and M. Ewing (1952). Two slow surface waves across North America, *Bull. Seismol. Soc. Am.* **42,** 219–228.

Rezaeian, S., and A. Der Kiureghian (2008). A stochastic ground motion model with separable temporal and spectral nonstationarities, *Earthq. Eng. Struct. Dyn.* **37,** 1565–1584.

Rezaeian, S., and A. Der Kiureghian, (2010). Simulation of synthetic ground motions for specific earthquake and site characteristics, *Earthq. Eng. Struct. Dyn.* **39,** 1155–1180.

Stolt, M. H., J. C. Baker, and T. W Simpson (1991). Characterization and genesis of saprolite derived from gneisses rocks of Virginia, *Soil Sci. Soc. Am. J.* **56,** no. 2, 531–539.

Tarr, A. C., and R. L. Wheeler (2006). Earthquakes in Virginia and vicinity 1774–2004, *U.S. Geol. Surv. Open-File Rept. 2006-1017*.

Wald, D. J., V. Quitoriano, T. H. Heaton, and H. Kanamori (1999). Relationship between peak ground acceleration, peak ground velocity, and modified Mercalli intensity in California, *Earthq. Spectra* **15,** no. 3, 557–564.

Wessel, P., and W. Smith (1991). Free software helps display data, *Eos Trans. AGU* **72,** 445–446.

Wessel, P., and W. H. F. Smith (2004). The Generic Mapping Tools (GMT) version 4 Technical Reference & Cookbook, SOEST/NOAA.

Wills, C. J., and W. Silva (1998). Shear wave velocity characteristics of geologic units in California, *Earthq. Spectra* **14,** 533–556.

Zeng, Y., J. G. Anderson, and F. Su (1994). A composite source model for computing realistic synthetic strong ground motions, *Geophys. Res. Lett.* **21,** 725–728.

U.S. Geological Survey
MS966, Box 25046
Denver, Colorado 80225
(D.E.M., H.M.B.)

U.S. Geological Survey
Albuquerque Seismological Laboratory
P.O. Box 82010
Albuquerque,New Mexico 87198-2010
(L.G.)

Department of Geosciences
4044 Derring Hall
Virginia Tech
Blacksburg, Virginia 24061
(M.C.)

Manuscript received 18 February 2013;
Published Online 14 January 2014